

Methods, Instrumentation and Mechanisms for Optical Characterization of Tissue and Treatment of Malignant Tumours

Sara Pålsson

Doctoral Thesis
Department of Physics
Lund Institute of Technology

Lund 2003

Copyright © 2003 Sara Pålsson
Printed at KFS AB, Lund, Sweden
February 2003

Lund Reports on Atomic Physics, LRAP-295
ISSN 0281-2162
LUTFD2(TFAF-1051)1-57(2003)
ISBN 91-628-5560-3

To Ulf and my Family

Contents

ABSTRACT

SAMMANFATTNING

LIST OF PAPERS

1	INTRODUCTION	1
2	INTERACTION OF LIGHT WITH TISSUE	3
2.1	PROPERTIES OF LIGHT	3
2.2	PROPERTIES OF ATOMS AND MOLECULES	4
2.2.1	<i>Energy levels in atoms and molecules</i>	4
2.2.2	<i>Transitions between levels</i>	7
2.3	THE INTERACTION OF LIGHT WITH TISSUE	8
2.3.1	<i>Absorption</i>	8
2.3.2	<i>Scattering</i>	9
2.4	MODELS FOR LIGHT DISTRIBUTION IN TISSUE.....	12
3	RAMAN SPECTROSCOPY FOR TISSUE CHARACTERIZATION	13
3.1	VIBRATIONAL TRANSITIONS IN TISSUE.....	14
3.1.1	<i>Proteins</i>	14
3.1.2	<i>DNA</i>	14
3.1.3	<i>Lipids</i>	15
3.1.4	<i>Differences in Raman signals from normal and malignant tissue</i>	15
3.1.5	<i>In vitro versus in vivo studies</i>	16
3.2	INSTRUMENTATION AND EVALUATION.....	16
3.2.1	<i>Excitation wavelength</i>	16
3.2.2	<i>Temperature considerations</i>	17
3.2.3	<i>Spectrographs</i>	17
3.2.4	<i>Detectors</i>	18
3.2.5	<i>Optical fibre probes</i>	18
3.2.6	<i>Background subtraction</i>	19
3.2.7	<i>Multivariate methods</i>	20
3.3	CLINICAL APPLICATIONS.....	21
3.3.1	<i>Cardiovascular applications</i>	21
3.3.2	<i>Oncological dermatology</i>	24
4	FLUORESCENCE SPECTROSCOPY FOR TISSUE CHARACTERIZATION .	27
4.1	AUTOFLUORESCENCE	27
4.1.1	<i>Collagen</i>	28
4.1.2	<i>Elastin</i>	28
4.1.3	<i>NADH/NAD+</i>	28
4.1.4	<i>Other fluorophores</i>	29

4.1.5	<i>Absorbers</i>	29
4.2	FLUORESCENT TUMOUR MARKERS	29
4.3	INSTRUMENTATION AND EVALUATION	31
4.3.1	<i>Diode fluorosensor</i>	31
4.3.2	<i>Spectral evaluation methods</i>	32
4.4	CLINICAL APPLICATIONS	33
4.4.1	<i>Cardiovascular</i>	33
4.4.2	<i>Skin</i>	34
4.4.3	<i>Cervix</i>	34
4.4.4	<i>Brain</i>	35
5	PHOTODYNAMIC THERAPY	37
5.1	PRINCIPLES OF ACTION	37
5.1.1	<i>Photosensitizers</i>	38
5.1.2	<i>Light</i>	38
5.1.3	<i>Oxygen</i>	39
5.1.4	<i>Dosimetry</i>	39
5.2	TREATMENT MECHANISMS	41
5.2.1	<i>Primary photodamage</i>	41
5.2.2	<i>Secondary effects</i>	41
5.3	CLINICAL APPLICATIONS	42
5.3.1	<i>Topical PDT of skin lesions</i>	42
5.3.2	<i>Interstitial PDT</i>	42

ACKNOWLEDGEMENTS

SUMMARY OF PAPERS

REFERENCES

Abstract

In this thesis, different optical methods utilising visible light for characterization of tissue have been developed and evaluated. The feasibility of many of these methods has been demonstrated in the laboratory or in animal experiments. However, the goal is naturally to develop methods useful in the clinic, and thus the emphasis in this thesis has been put on *in vivo* examinations.

Raman spectroscopy is an optical method that can provide information regarding vibrational modes in molecules and concentrations of tissue constituents. The Raman spectra contain sharp peaks and are suited for multivariate evaluation since one specific peak represents a vibrational mode that can be present in many different molecules. The Raman signal is weak and is often hidden in the strong fluorescence emission from tissue. The main challenge lies in the development of clinical Raman spectroscopy systems that are capable of recording Raman spectra with high resolution and low noise in a short accumulation time. This problem is discussed together with applications of Raman spectroscopy in cardiology and dermatology.

Fluorescence spectroscopy is another technique used for tissue characterization and detection of lesions. The application of fluorescence spectroscopy for the delineation of borders between normal and malignant tissue in oncological dermatology and neurosurgery is discussed as well as the potential of classification of myocardial biopsies from patients with transplanted hearts. The construction and usefulness of a small clinical system is also discussed. In the development of models capable of correlating fluorescence spectra with clinical diagnosis, the problem of biopsy location and biological variability within the biopsies has been addressed in a study of protocols for histopathological evaluation in the field of gynaecology.

The use of light for treatment of malignant tumours is often associated with the thermal impact of laser 'knives' employed during excisions. However, light can also be a constituent in non-thermal photochemical reactions where light, together with a tumour-seeking photosensitizer and tissue oxygen, react and lead to cell death, which kills tumours. This treatment modality is called photodynamic therapy and some of the involved mechanisms have been explored in the thesis. Due to the limited penetration of visible light, a system for interstitial delivery of treatment light has been developed to be able to treat thicker and deeply located tumours. The dosimetry is important and the photodynamic threshold dose has been estimated.

Sammanfattning

Denna avhandling handlar om hur ljus kan användas för att detektera, diagnosticera och behandla olika medicinska sjukdomstillstånd. Det vi dagligen kallar ljus är bara en liten del av det elektromagnetiska spektret, nämligen den del vi kan uppfatta med våra ögon. Elektromagnetisk strålning med andra våglängder används i stor utsträckning för klinisk diagnostik. Röntgenstrålning, mikrovågor och gammastrålning är andra exempel på strålning som används för behandling av olika sjukdomstillstånd, men det är det synliga ljusets interaktion med vävnad som denna avhandling handlar om.

Genom att sända in ljus i vävnad och med hjälp av känsliga ljusdetektorer mäta ljuset som kommer tillbaka kan man få kunskap om vävnadens ämnesinnehåll och på så sätt göra en diagnos. Lasrar är praktiska att använda då dessa har en väldefinierad emissionsvåglängd (färg), en hög uteffekt och ljusstrålen utbreder sig rätlinjigt i en smal stråle. Ljus från en laser går lätt att sända in i tunna optiska fibrer och på så sätt kan man mäta i hålrum inuti kroppen genom endoskop och nålar. De ljusenergier som används är små och leder inte till någon nämnvärd uppvärmning av vävnaden. Istället är det ljusets interaktion med molekylernas energinivåer som är det intressanta.

Alla har vi någon gång försökt lysa genom handen med en vanlig ficklampa. Då kan man observera två fenomen; man ser inga skuggor av ben i handen och ljuset som kommer ut är rött. Vävnad består av celler vars cellmembran och inre organeller fungerar som små ytor där ljus kan reflekteras och byta riktning. Synligt ljus (till skillnad från röntgenstrålning) studsar omkring i vävnad och på andra sidan handen kommer ljuset ut diffust. Detta fenomen kallas för spridning och vävnad, i likhet med dimma, moln och mjölk, benämns som ett spridande material.

Vid vanlig (elastisk) spridning bevaras ljusets energi och det spridda ljuset har samma våglängd som det inkommande. Det finns även en mer sällsynt spridningsprocess, Ramanspridning, då det spridda ljusets våglängd förändras något då ljuset sprids mot en vibrerande eller roterande molekyl. Genom att analysera energiskiftet i det spridda ljuset, kan man få information om vilka vibrations- och rotationsenergier som finns. Från dessa energier kan man dra slutsatser om molekylerna som ingår i vävnaden vilket ger en uppfattning om vävnadstyp. Denna metod beskrivs i avhandlingen och ett mobilt system har konstruerats för kliniska studier. Mätningar har utförts på patienter för att försöka särskilja olika typer av hudtumörer och i syfte att undersöka om man kan karakterisera de ingående molekylerna i hjärt- och kärlvävnad.

Hemoglobin är det protein i de röda blodkropparna som transporterar syre från lungorna ut till resten av kroppen. Det är en stark absorbator som tillsammans med melanin (hudens pigment) och andra svagare absorbatorer absorberar grönt och blått ljus vilket leder till att ljuset ser rött ut på andra sidan handen.

En del ämnen har förmåga att fluorescera, dvs. sända ut synligt ljus i olika färger då de belyses med osynligt ultraviolett eller blått ljus med kort våglängd. I vävnad finns det ett fåtal molekyler som har denna förmåga, bl a kollagen, elastin, NADH, β -karoten, tryptofan och porfyriner. Genom att analysera fluorescensen från vävnad kan man se skillnader mellan olika vävnadstyper. Inom ramen för avhandlingen har utrustning för att mäta vävnadsfluorescens konstruerats och utvärderats. I avhandlingen har studier för att skilja tumörer i huden, på livmoderhalstappen och i hjärnan från normal vävnad utförts. Studier för att se skillnad på avstött hjärtvävnad från normal hjärtmuskel hos personer med transplanterat hjärta har genomförts och även försök att karakterisera olika grader av åderförkalkning i kärlvävnad.

Både Raman och fluorescensspektroskopi är potentiella optiska metoder som utan att orsaka skada kan diagnosticera vävnad i realtid. De kan används för tidig detektion av pre-cancerogena förändringar och som hjälp vid biopsitagning i vävnader där det inte är uppenbart var man skall ta vävnadsprov för mikroskopisk analys, t ex i lungan eller i urinblåsan. Avbildande fluorescens system är till stor hjälp i de fall där en biopsitagning tar bort viktig vävnad, t ex vid stämbandscancer.

Genom att ge patienterna en viss aminosyra, ALA, kommer stora mängder av ett fluorescerande ämne, protoporphyrin IX (PpIX), att ansamlas i högre grad i malign vävnad än i normal på grund av enzymatiska skillnader. Då PpIX fluorescerar starkt i rött är det lätt att skilja den från den blå-gröna fluorescensen från vävnadens egna molekyler. På så sätt blir cancerdetektionen mer känslig.

PpIX kan även användas för behandling av tumörer. ALA ges då i en större dos och efter 3-4 timmar kan patienten behandlas. Området belyses vid behandling med en röd laser med samma våglängd (635 nm) där man tidigare mätte fluorescensen, och energin absorberas då av PpIX. Energin omfördelas i PpIX så att dess energitillstånd matchar en energiövergång i syre som finns i vävnaden. Vid kollision överförs energin och syret blir en syreradikal som oxiderar allt i sin närhet. Då PpIX finns i cellens membran går dessa sönder och cellen dör. Efter detta förlopp är PpIX i sitt ursprungstillstånd och kan absorbera nya ljusfotoner. Hela processen är fotokemisk och benämns fotodynamisk tumörterapi eller Photodynamic Therapy (PDT). Då PpIX ansamlas i större grad i tumörvävnad än i normal, är behandlingen selektiv och man kan alltså belysa ett stort område och ändå bara döda tumörceller.

En del av avhandlingen är studier av de olika mekanismerna som finns vid PDT. Då hudtumörer behandlas genom att belysa vävnaden från ytan med laserljus har mätningar gjorts av hudens temperatur med hjälp av en värmekamera. Även om patienten kan uppleva PDT behandlingen som brännande och stickande är det i princip ingen värme inblandad eftersom det är en rent kemisk process. En liten del av behandlingsljuset absorberas av hudens melanin men ger alltså inte upphov till någon nämnvärd värme. För att PDT skall fungera krävs det syre som transporteras ut i vävnaden med blodet. Mätningar har gjorts med ett svepande lasersystem som mäter Doppler skiftet på en del av ljus som reflekteras mot blodkroppar i rörelse. Man kan då erhålla en bild över blodflödet i tumören och utanför. Mätningar utfördes före,

direkt efter och en timme efter behandlingen, och intressanta skillnader uppvisades.

Som beskrivits ovan, är det röda behandlingsljusets inträngningsdjup i vävnad begränsad till ett par millimeter. För att kunna behandla tjockare tumörer och tumörer inbäddade i vävnad, har system för interstitiell PDT (IPDT) utvecklats. Ljuset skickas genom tunna optiska fibrer som sätts in i vävnaden med hjälp av nålar. På så sätt kan en större tumörmassa behandlas. För att kontrollera behandlingen krävs en god kunskap om dosimetrin, dvs hur ljuset fördelar sig. Experimentella försök har gjorts på råttor med inplanterade tumörer på bakbenen, för att få kunskap om den ljusdos och koncentration av det sensibiliserande ämnet som krävs för att vävnaden skall dö. Tekniken har även används vid klinisk behandling av tjocka tumörer.

List of Papers

This thesis is based on the following papers:

- I. S. Pålsson, N. Bendsoe, K. Svanberg, S. Andersson-Engels and S. Svanberg, NIR Raman spectroscopy for in vivo characterization of skin lesions, Submitted to Photochemistry and Photobiology (2003).
- II. J. Swartling, S. Pålsson, P. Platonov, B. Olsson and S. Andersson-Engels, Changes in tissue optical properties due to radio frequency ablation of myocardium, Resubmitted to Medical and Biological Engineering and Computing, after minor corrections (2003).
- III. S. Pålsson, S. Yuan, B. Kornhall, M. Block, L. Johansson, B. Olsson and S. Andersson-Engels, Laser-induced fluorescence examination of myocardial biopsies in patients with transplanted hearts, Submitted to Journal of Biomedical Optics (2002).
- IV. U. Gustafsson, S. Pålsson and S. Svanberg, Compact fibre-optic fluorosensor using a continuous wave violet diode laser and an integrated spectrometer, Rev. Sci. Instrum. **71**, 3004-3006 (2000).
- V. S. Pålsson, E.-O. Backlund, O. Eriksson, P. Lundberg, P. Sturnegk, K. Wårdell, K. Svanberg and S. Andersson-Engels, ALA-PpIX fluorescence spectroscopy studied during stereotactic biopsy of human glioblastomas, Manuscript in preparation (2003).
- VI. S. Pålsson, U. Stenram, M. Soto Thompson, A. Vaitkuvienė, V. Puskiene, R. Ziobakiene, J. Oyama, U. Gustafsson, M.J. DeWeert, N. Bendsoe, S. Andersson-Engels, S. Svanberg and K. Svanberg, Methods for detailed histopathological investigation and localisation of cervical biopsies to improve the interpretation of autofluorescence data, Submitted to Lasers in Surgery and Medicine (2003).
- VII. U. Gustafsson, E. McLaughlin, E. Jacobson, J. Håkansson, P. Troy, M.J. DeWeert, S. Pålsson, M. Soto Thompson, S. Svanberg, A. Vaitkuvienė and K. Svanberg, Fluorescence and reflectance monitoring of human cervical tissue in vivo - A case study, in Spectral Imaging: Instrumentation, Applications and Analysis, Proc. SPIE **4959-12**, To appear (2003).

- VIII. M.J. DeWeert, J. Oyama, E. McLaughlin, E. Jacobson, J. Håkansson, G.S. Bignami, U. Gustafsson, P. Troy, V. Poskiene, K. Kriukelyte, R. Ziobakiene, A. Vaitkuviene, S. Pålsson, M. Soto Thompson, U. Stenram, S. Andersson-Engels, S. Svanberg and K. Svanberg, Analysis of the spatial variability in hyperspectral imagery of the uterine cervix in vivo, in *Spectral Imaging: Instrumentation, Applications and Analysis*, Proc. SPIE **4959-08**, To appear (2003).
- IX. M. Soto Thompson, L. Gustafsson, S. Pålsson, N. Bendsoe, M. Stenberg, C. af Klinteberg, S. Andersson-Engels and K. Svanberg, Photodynamic therapy and diagnostic measurements of basal cell carcinomas using esterified and non-esterified δ -aminolevulinic acid, *J. Porphyrins Phthalocyanines* **5**, 147-153 (2001).
- X. S. Pålsson, L. Gustafsson, M. Soto Thompson, M. Stenberg, N. Bendsoe, S. Andersson-Engels and K. Svanberg, Kinetics of the superficial perfusion and temperature in connection with photodynamic therapy of basal cell carcinomas using esterified and non-esterified 5-aminolevulinic acid, *British Journal of Dermatology*, In press (2003).
- XI. I. Karu, S. Pålsson, I. Wang, C. af Klinteberg, N. Bendsoe, S. Andersson-Engels, S. Svanberg and K. Svanberg, Photodynamic therapy using δ -amino levulinic acid and intensity modulated diode laser light, Manuscript in preparation (2003).
- XII. S. Pålsson, L. Gustafsson, U. Stenram, M. Soto Thompson, S. Svanberg, K. Svanberg and S. Andersson-Engels, Estimation of the protoporphyrin IX photodynamic threshold dose, Submitted to *Photochemistry and Photobiology* (2003).
- XIII. M. Stenberg, M. Soto Thompson, T. Johansson, S. Pålsson, C. af Klinteberg, S. Andersson-Engels, U. Stenram, S. Svanberg and K. Svanberg, Interstitial photodynamic therapy - diagnostic measurements and treatment in malignant experimental rat tumours, in *Optical Biopsy and Tissue Optics*, eds. I.J. Bigio, G.J. Mueller, G.J. Puppels, R.W. Steiner and K. Svanberg, Proc. SPIE **4161**, 151-157 (2000).
- XIV. M. Soto Thompson, T. Johansson, S. Pålsson, S. Andersson-Engels, S. Svanberg, N. Bendsoe, U. Stenram, K. Svanberg, J. Spigulis, A. Derjabo and J. Kapostins, Photodynamic therapy of basal cell carcinoma with multi-fibre contact light delivery, Submitted to the *British Journal of Dermatology* (2003).

1 Introduction

The vision is perhaps the most important sense of humans for the interpretation of the environment we live in. The ability to detect and interpret electromagnetic radiation into shapes and colours is resulting in pattern recognition and awareness after processing by the brain. In the field of medicine, the visual examination of a patient provides information that can be used to suggest the diagnosis by interpretation of colours, textures and shapes of suspicious malignant conditions. Radiation in other wavelength ranges, invisible to the eye, is widely used in X-ray imaging, CT scans, MR imaging and isotopes detection. In this thesis, visible light has also been used for the characterization of tissue; however, the visual perception by the eye has been replaced by light sensitive detectors. Basically, light is sent into the tissue and the light that returns is detected and interpreted in terms of tissue constituents, which provide indication on the tissue type and diagnosis. Visible light can also be utilised for the treatment of malignant tumours. The process (photodynamic therapy, PDT) is non-thermal and involves photochemical reactions, which lead to selective tumour destruction.

This thesis deals with the optimisation of optical spectroscopical techniques for tissue characterization and comprises development of systems and methods for Raman and fluorescence spectroscopy together with the evaluation in several clinical trials in various specialities. Some of the mechanisms of PDT have been investigated in the thesis and a system for treatment of massive tumours has been tested experimentally and clinically.

2 Interaction of light with tissue

This thesis focuses on the use of fluorescence and Raman spectroscopy to characterise tissue and provide methods for optical medical diagnostics. Photodynamic therapy is a method to treat malignant tissue and some of the action mechanisms have been investigated. None of these processes involve any heat formation, which often is associated with the use of lasers in medicine. Instead, the mechanisms are of photochemical nature, involving energy exchange between the quantised levels of atoms and molecules present in tissue.

To fully understand the principles of the interaction of light with tissue, an overview of the general properties of light and molecules is given in this chapter before the specific tissue-light interactions are described.

2.1 Properties of light

Light is dualistic in nature. It can be described as an electromagnetic wave or as a package or quantum of energy - a photon. The aspects are equally valid and often one or the other is chosen to describe a specific phenomenon. The electromagnetic spectrum ranges from radio waves through infrared and visible light to X-rays and gamma radiation. The wavelength, λ , or the frequency, ν , are used to describe the radiation when the wave nature is considered, and the energy, E , is used when light is regarded as a stream of photons. These quantities are easily connected by the speed of light, c , and the Planck constant, h .

$$E = h \cdot \nu = h \cdot \frac{c}{\lambda} \quad [\text{J}] \quad c = \lambda \cdot \nu \quad [\text{m/s}]$$

In the experiments described in this thesis, light in the visible and near infrared range has been used. In this region, the wavelength, λ , is the most common quantity used to represent the light energy. In the field of Raman spectroscopy, energy differences are often described in wave numbers, σ , which can be calculated as:

$$\sigma = \frac{1}{\lambda_1} - \frac{1}{\lambda_2} \quad [\text{cm}^{-1}]$$

The advantage of this approach is that wave numbers are directly proportional to energy.

The light fluence rate is another important parameter. It can be represented in many ways and by many symbols, but the one used in this thesis is ϕ , which often is expressed in mW/cm^2 . The unit can be considered as the light energy per second passing through the cross section area of an imaginary infinitesimal sphere.

2.2 Properties of atoms and molecules

During the first decades of the 20:th century, the theories of atomic physics and quantum mechanics were developed by Bohr, Schrödinger and others. These early theories are fully capable of describing energy levels and transitions in atoms and molecules, and only the fundamentals are required for the understanding of this thesis. Quantum mechanics and atomic physics have continued to develop and for a more detailed description, the reader is referred to textbooks, e.g. Refs^{1,2}.

2.2.1 Energy levels in atoms and molecules

The hydrogen atom with one electron circulating around the charged nucleus is the simplest atomic system. Solutions to the Schrödinger equation in a Coulomb potential yield electronic states. The energy of these states can be calculated by the use of the Rydberg formula and the primary quantum number, n . For all other atoms, the interaction between multiple electrons and the interaction between electrons and the angular momentum give rise to the need of additional quantum numbers to describe the energy levels³.

According to the Pauli exclusion principle, there cannot be more than two electrons occupying any state, one with electronic spin up and one with spin down. Basically, the states of the atom are filled from the lowest state and upwards. The configuration of electrons in various shells is described by many parameters, for instance triplet and singlet states. There are several quantum mechanical rules that determine allowed transitions between electron configurations. In Fig. 1, a schematic picture of energy levels in a hydrogen atom is shown.

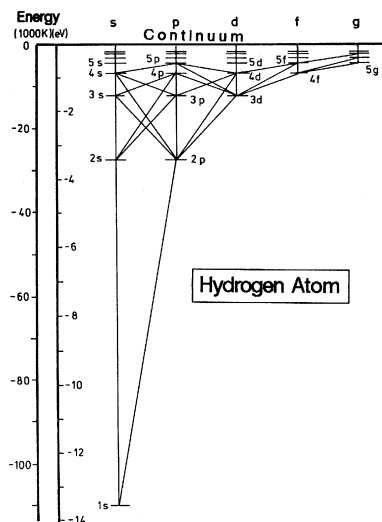


Figure 1. Energy levels of the hydrogen atom. The numbers 1,2,3 etc are the principal quantum numbers and s,p,d etc. corresponds to the subshells. The lines between the levels indicate allowed transitions. Taken from Ref.³.

The distribution of atoms in specific states is described by Boltzmann's law

$$\frac{N_1}{N_2} = e^{\frac{h\nu}{kT}},$$

where N_1 and N_2 is the number of atoms in two different states (N_1 is the lower lying state), $h\nu$ is the energy difference between the states, T is the absolute temperature and k is the Boltzmann constant. For an electronic transition in the visible range (typically $\lambda=500$ nm, $T=300$ K), the exponent is about 100 and thus practically all atoms are in the ground state.

When atoms bond together to form molecules, the total energy is lower than the sum of energy of the constituents. The description of energy levels becomes more complicated than for atoms, since energy states due to vibration and rotation motion are added. In Fig. 2, the schematic picture of electronic levels and the addition of vibration and rotation levels is shown.

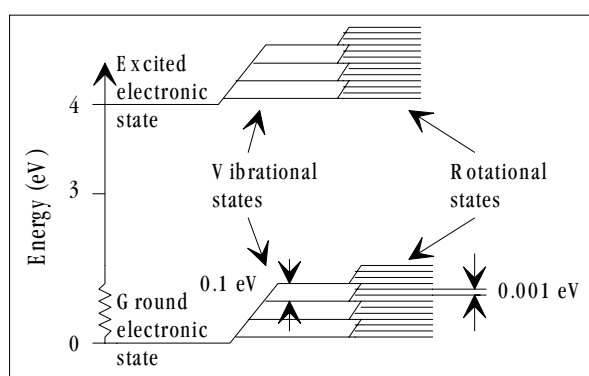


Figure 2. Energy states in a molecule. Modified from Ref.³.

The simplest calculation of vibrational energy levels for a diatomic molecule involves the approximation of the potential by a parabola as in a harmonic oscillator. This results in a simple expression of vibration frequency and energy

$$E_v = (v + \frac{1}{2})h\nu_c \quad v = 0, 1, 2, \dots,$$

where ν_c is the classical vibrational frequency given by the expression

$$\nu_c = \frac{1}{2\pi} \sqrt{\frac{k}{\mu}},$$

where μ is the reduced mass and k is a force constant. Thus, the vibrational levels are equidistant and there will always be a non-zero lowest vibrational energy.

The degree of complexity increases for polyatomic molecules and there can be numerous modes of vibration. An atom has 3 degrees of freedom and put together in a molecule, an N-atomic molecule has 3N degrees of freedom. The translation directions and rotation around the mass centre are not vibrations; thus there can be 3N-6 vibration modes for an N-atomic molecule.

There are two types of vibrational modes: stretching modes, where the distances between the atoms or groups of atoms are altered; and bending modes, where the angles between atoms or groups of atoms are altered. Some examples of vibrational modes can be seen in Fig. 3.

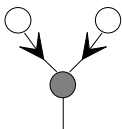
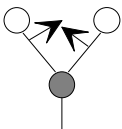
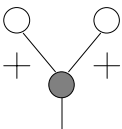
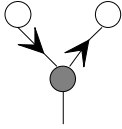
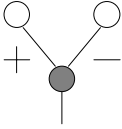
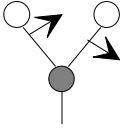
Stretching	Bending	
 <p>Symmetric</p>	 <p>Scissoring</p>	 <p>Wagging</p>
 <p>Asymmetric</p>	 <p>Twisting</p>	 <p>Rocking</p>

Figure 3. Vibrational modes for atoms or groups of atoms. The + and - signs indicate movement out of and into the plane of this page. Modified from Ref.³.

Molecules in general can rotate around three different axes. For the simple case of a diatomic molecule, it rotates around the mass centre and the rotation energy can be calculated as

$$E_J = BJ(J+1) \quad J = 0, 1, 2, \dots,$$

with

$$B = \frac{\hbar^2}{2I},$$

where I is the moment of inertia with respect to the rotation axis. If the bond between the atoms is not completely rigid, the molecular bond will be stretched out in higher rotational states and I will increase, leading to a downshift of higher levels. In polyatomic molecules the theory becomes much more complex, and also here symmetry aspects are important. In large biomolecules, the rotational structure, in the energy level diagram, is often lost and the energy levels are smeared out into a band.

2.2.2 Transitions between levels

The configuration of the energy levels of a molecule determines many of the properties of that molecule. For instance, the energy separation between the electronic states determines the visible wavelengths that can be absorbed and thus the colour of the molecule. The transitions between the levels are the origin of many interesting phenomena like laser action, phosphorescence and fluorescence.

The energy separations between close-lying electronic levels often correspond to visible wavelengths. Vibration transitions occur in the infrared range, while transitions between rotational levels in the same vibrational mode fall in the far infrared range. There are rules for radiative transition within vibration and rotational levels. For vibration, $\Delta v = \pm 1$ must be fulfilled and for rotation $\Delta J = \pm 1$.

Light impinging on a molecule can, if the energy corresponds to the energy separation between two levels, be absorbed and an electron is transferred to a higher level. The molecule only remains in this state for a short period of time given by the lifetime of that state. On the way back to the ground state, none or several intermediate levels may be involved. However, there are some restrictions on the possible transitions between energy levels, set by the selection rules of quantum mechanics.

The transition between a singlet and a triplet state including emission of light is forbidden, since the electron spin cannot be changed in such a process. If an atom, with a singlet ground state, is in its lowest lying triplet state, it can only release the excess energy due to other interactions, for instance collisions. Such a transition is called inter-system crossing. Thus the triplet state is a metastable state with a long lifetime. In a so-called Jablonski diagram, Fig. 4, the transition from state S_1 to T_1 is shown. In this state, the molecule can stay for long times since the transition to the ground state S_0 is forbidden. If it returns to the ground state, the emission is called phosphorescence.

There are several ways for an atom to return to its ground state from an excited state. Due to interaction with other molecules, the electron is transferred to the lowest lying vibrational and rotational state within the excited state. This is called internal conversion. When the molecule returns to any of the levels in the ground state, fluorescence light can be emitted. The wavelength of the fluorescence will always be longer than the excitation light. Fluorescence light in solids and liquids is broad-banded due to the strong interaction between molecules and due to the large number of vibration and rotation levels. The excited molecule can also return non-radiatively through collisions and internal conversion. Together with inter-system crossing, these possibilities compete with fluorescence emission.

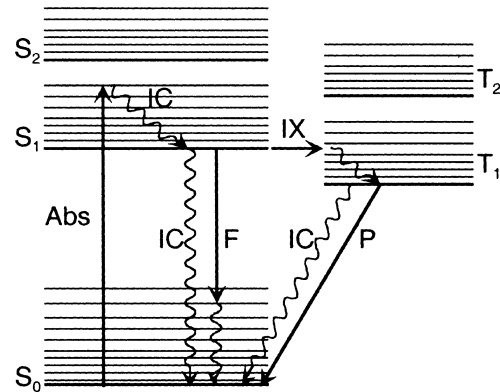


Figure 4. Jablonski diagram showing the absorption of a photon and some of the possible relaxation processes. IC, internal conversion; F, fluorescence; IX, intersystem crossing; P, phosphorescence. Taken from Ref.⁴.

The time an average electron stays in a specific energy level is called the lifetime. The natural radiative lifetime of a free atom or molecule is a result of quantum mechanics, which can be expressed by the Heisenberg uncertainty principle. The lifetime may be drastically shortened by collisions.

2.3 The interaction of light with tissue

In the previous chapter, the general features of light and molecules were described. In this chapter the focus is on the interaction between light and the cells and molecules present in tissue.

2.3.1 Absorption

Light incident on tissue can be absorbed by various chromophores. The absorption coefficient, μ_a , is the parameter used to describe the probability of absorption. It is defined as the probability of absorption per unit length and is normally expressed in cm^{-1} . The absorption of light in tissue is strongly dependent on wavelength. In Fig. 5, the absorption spectra of the most abundant absorbers in tissue can be found. Haemoglobin and melanin absorb strongly in the blue and UV ranges, while water is the strongest absorber in the infrared range.

As can be seen, some of the absorbers have absorption spectra with prominent peaks. In the wavelength region between 650 - 1300 nm, the total absorbance is the lowest. This region is called the tissue optical window since it is in this region of the visible/NIR range where tissue is most transparent.

After absorption, the energy can be released by emission of light (fluorescence and phosphorescence) or the molecules can be non-radiatively transferred back to the ground state. Fluorescence emission is further discussed in Chap. 4.

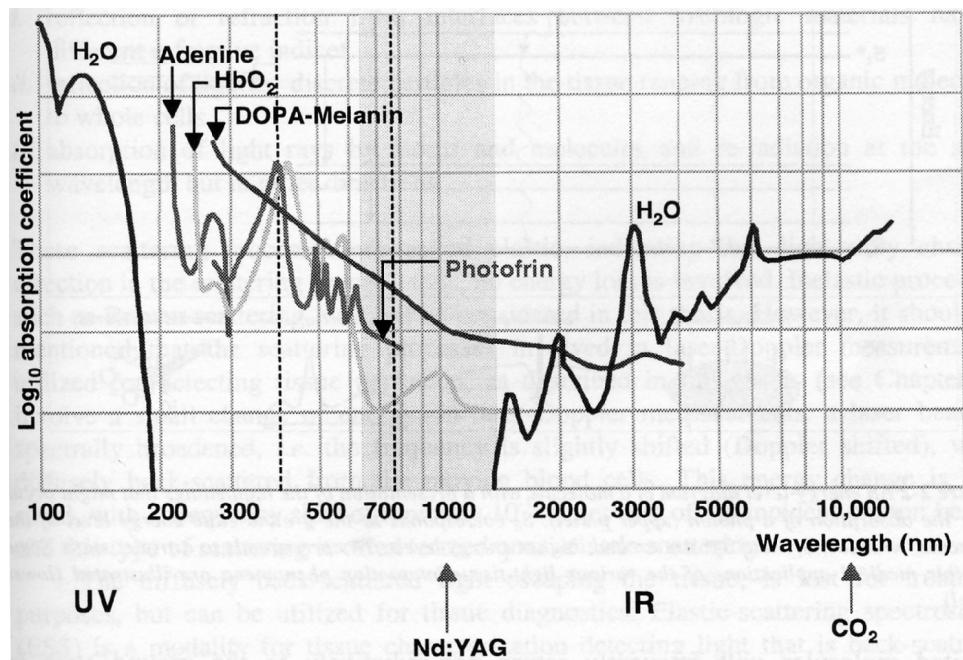


Figure 5. The absorption coefficient is plotted versus wavelength for the major absorbers in tissue and in addition the absorption spectrum of Photosfrin, a photosensitizer drug commonly used for photodynamic treatment of tumours is given. The dotted lines indicate the limits of the visible range. The grey area corresponds to the wavelength range where the total absorption is low. The region is referred to as the tissue optical window. The emission wavelengths of the Nd:YAG and CO₂ lasers are indicated. Figure adopted from Boulnois⁵.

The energy absorbed in a molecule can also generate heat, which can be used as a treatment modality in itself^{6,7}. In between 41-47°C, malignant tissue is slightly more sensitive to heat than healthy tissue^{8,9} and this can be used for selective treatment. Above that temperature interval, all tissue is equally sensitive and at 60°C, the proteins are coagulated. For all these methods, a feed-back control of tissue temperature for treatment monitoring is crucial, since the cooling blood perfusion can vary substantially.

2.3.2 Scattering

Light incident on tissue will be scattered around and rather than travel in straight paths. This scattering is called elastic, since there is no energy loss, only a change in direction.

Macroscopically, tissue has a refraction index of about $n = 1.4^{10}$ and some of the light incident on a tissue surface will be reflected according to the Snell law. However, on the microscopic scale, tissue is highly inhomogeneous with a varying refraction index. Tissue is thus highly scattering and it is also called turbid media. The cell nucleus, the membranes of the cells¹¹ and cell organelles like mitochondria¹², lysosomes and the

Golgi apparatus are considered to be the dominant scatterers together with lipid vesicles in fatty tissue.

There are two types of elastic scattering; Rayleigh and Mie scattering. If the size of the scatterers is considerably larger than the wavelength, the light will be Mie scattered. Strict Mie theory refers to spherical particles, but generalisations can be made. The probability of Mie scattering is a very complex function of wavelength, the refraction indices of the particle and the surrounding medium, and the probability for absorption. In general, the intensity of the scattered light increases with shorter wavelengths and follows approximately a λ^{-2} dependence.

Rayleigh scattering occurs when non-resonant light interacts with scatterers smaller than the wavelength, for instance molecules. The varying electric field creates a polarisation in molecules, which act like antennas and re-emit the light in a new direction. The probability for Rayleigh scattering increases with shorter wavelengths and follows a λ^{-4} dependence.

If the incoming light interacts with vibration and rotation levels of molecules and cause a transition between such levels, the scattering will be inelastic, since the scattered light has a different wavelength (energy) than the incoming light. If the energy of the incoming light does not match the electronic level energy separation, then Rayleigh and Raman scattering can occur. In these cases the molecule is excited to a virtual level and from there, light may be emitted. Depending on the initial and final states, energy is gained, preserved or lost. If it is preserved, it is called Rayleigh scattering. If energy is lost or gained we talk about Stokes and Anti-Stokes Raman scattering, respectively. The energy of vibration modes is normally expressed in wavenumbers. Since the Raman vibration energy is calculated as the difference in wavenumber of the excitation and emission, and since wavenumbers are proportional to energies, Raman spectra recorded with different systems and thus excitation wavelengths, can be compared directly. A summary of scattering processes involving the electronic states can be found in Fig. 6. Raman spectroscopy is further discussed in Chap. 3.

The scattering coefficient, μ_s , is used to describe scattering in turbid media. It is defined as the probability of scattering per unit length and is often given in inverse centimetres, cm^{-1} . The wavelength dependence of the scattering coefficient in tissue is not as strong as for absorption. Scattering in tissue is not isotropic, but strongly forward directed. The scattering anisotropy is often described by the g-factor, which is related to the average scattering angle by the relation

$$g = \langle \cos(\theta) \rangle .$$

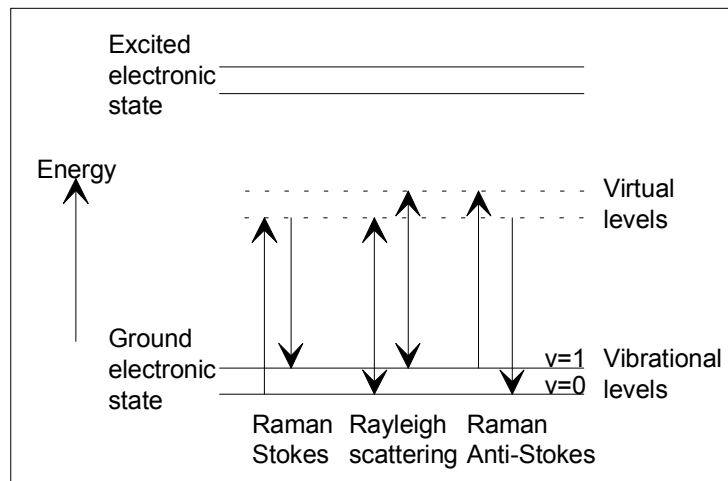


Figure 6. Raman scattering.

The reduced scattering coefficient defined as

$$\mu'_s = \mu_s(1 - g)$$

is a measure of the effective mean free path between two scattering events for an assumed case where all scattering events are isotropic (i.e. $g = 0$). It can thus be interpreted as the inverse of the average distance a photon travels before the accumulated resulting scattering effect can be considered isotropic. The reduced scattering coefficient is very useful in tissue optics, since many methods, which measure tissue optical parameters, only measure the reduced scattering coefficient. The g -factor and the scattering coefficient cannot be separated once the light is scattered a sufficient number of times to be considered diffuse.

By sending in light into tissue and detect the emerging light, the scattered light might be useful for diagnostic purposes. The multiple scattered light is sensitive to tissue absorbers and to the size of scattering structures, such as cell organelles. These may be different in malignant as compared to healthy tissue. The method can be performed both with continuous light utilising optical detection fibres located at fix distances from the source fibre, usually referred to as diffuse reflectance spectroscopy¹³ or elastic scattering spectroscopy^{14,15}; or with time resolved techniques¹⁶⁻¹⁹.

Light incident on tissue may also scatter towards moving objects like blood cells. By measuring the Doppler frequency shift of the scattered light, the perfusion can be imaged using a scanning instrument²⁰. This type of instrument was employed in Paper X for the measurement of superficial blood perfusion during photodynamic therapy.

2.4 Models for light distribution in tissue

In some of the work presented (Paper XII), an analytical expression has been used to calculate the light distribution in tissue when light is injected from an optical fibre inserted into the tissue. Using the diffusion approximation²¹, the expression for the fluence rate becomes

$$\phi = \frac{P_0 \mu_{eff}^2}{4\pi \mu_a r_n} e^{-\mu_{eff} r_n} \left[\frac{W}{cm^2} \right]$$

at a distance r_n away from the source. The equation originates from the radiative transport theory, which is a model to describe the light fluence in terms of individual particles that travel straight until scattered or absorbed. Since most of the wave characteristics of light like polarisation and interference phenomena etc. are lost when light travels through tissue, this model with light considered as a stream of individual particles with an individual quantum of energy is adequate. The diffusion theory is an approximate solution and it is valid when the scattering is much stronger than absorption, typically expressed as $\mu_s(1-g) \gg \mu_a$.

Numerical methods like Monte Carlo^{22,23} and the adding doubling method²⁴ can also be used for calculating the light distribution in tissue.

3 Raman spectroscopy for tissue characterization

Raman spectroscopy probes the vibration modes of molecules in a sample and the resulting spectrum contains multiple narrow peaks, which correspond to specific vibrational modes of the molecules and provide direct information on the biochemical composition. The peaks are narrow, and sensitive to molecular concentration, structure, conformation and environment, and taken together, all different peaks from a molecule provide a spectral ‘fingerprint’.

Almost all molecules exhibit Raman scattering. However, Raman scattered light is weak and it is often hidden in the fluorescence emission. Together with a possible requirement of using fibre optics to access not only the skin, but also other tissues inside the body, complicated and expensive instrumentation is needed for medical characterization of various tissue types.

The discovery of the Raman scattering process has been attributed to the Indian physicist C.V. Raman, who in 1928 observed a new scattering process. Raman spectroscopy was not extensively employed as an analytical tool until the invention of the laser in 1960. Raman spectroscopy was first adopted by the chemists to study chemical analytes. The early attempts to measure Raman spectra of cells and tissue were obstructed by the facts that there was no way to suppress the fluorescence and that the instruments had a limited performance. The first Raman spectra from tissue were reported in 1988 by Clarke *et al.*²⁵ and in 1989 by Alfano *et al.*²⁶. Raman studies of biological tissue have been facilitated over recent years by advancing technology, particular in the areas of lasers and detectors. To get a real success of providing insight into the molecular basis of a disease and showing the potential for medical diagnostic applications, the methods for analysing Raman spectra should rely on the full Raman spectra, not just the prominent peaks, in order to extract useful reliable diagnostic information. Thus, there is a great interest in different multivariate techniques for evaluating Raman spectra.

Today, Raman spectroscopy is still mostly used in the field of chemistry, and Raman spectroscopy for medical applications is in the proof-of-concept stage. The potential of Raman spectroscopy for tissue characterization and diagnostics has been reviewed²⁷⁻²⁹ and requirements for the clinical implementation are discussed in Ref.³⁰.

3.1 *Vibrational transitions in tissue*

In the following sections, the origin of tissue Raman peaks is discussed and the presentation largely follows the discussion given in Refs^{27,29}.

3.1.1 **Proteins**

Proteins give rise to many vibrational modes and many Raman peaks originate from the amide (peptide) bond linking the amino acids to form the protein. The exact location of these peaks (the energy of the vibrational mode) is dependent on the secondary structure of the protein, i.e. the three-dimensional structure.

Various amino acids can be characterised by their vibrational peaks, e.g. tyrosine (830 and 850 cm^{-1}), tryptophan (1014, 1338, 1361 and 1553 cm^{-1}), and phenylalanine with a peak at 1006 cm^{-1} . The secondary protein structure significantly influences the Raman spectrum of the peptide backbone. The amide linkage between amino acid residues has four normal modes, two of which are active in Raman scattering, the amide I and III modes. The amide I mode is largely due to C=O stretching and the amide III mode is due to C-N stretching and N-H in plane bending. The positions of the amide I and amide III peaks as well as the skeletal C-C vibrations near 900-980 cm^{-1} can be used to characterise the secondary structure of proteins.

The C-H deformation vibration mode at 1448 to 1459 cm^{-1} originates from methylene groups and the peak intensity is relative insensitive to conformation and can be used as an intensity standard. Disulfide bridges, which are important in tertiary structure of a protein, exhibit Raman signals at 500 to 550 cm^{-1} .

Collagen and elastin are the principal structural proteins of human tissue. For instance, collagen shows a strong amide I peak (1650 cm^{-1}) and two amide III bands at 1271 and 1248 cm^{-1} which attribute to amide vibrations in the polar (proline-rich) and non-polar (proline-poor) regions of the triple helix conformation²⁷. Elastin shows strong amide III (1250 cm^{-1}) and amide I (1660 cm^{-1}) vibrations and weak skeletal C-C spectral feature characteristic of disordered protein conformations.

The bands at 1108, 966 and 529 cm^{-1} are not present in collagen nor in globular proteins and have been attributed to its unique amino acids, desmosine and isodesmosine.

3.1.2 **DNA**

Nucleic acids, such as DNA, are built from nucleotids, which consist of a phosphorylated sugar attached to a purine (adenine or guanine) or pyrimidine (cytosin or thymine) base. Hydrogen bonds between complementary base pairs together with additional interaction between bases along the axis stabilise the double-stranded helical forms of DNA. The B-form of DNA corresponds to a right-handed helix and is the most abundant form of DNA. It has been shown that Raman spectroscopy can be used to determine the conformation of DNA and also probe subtle changes in the B form.

In general, vibrations of either the sugar backbone or the bases give rise to Raman peaks. Vibration in the cyclic rings within the bases gives rise to several peaks in the regions $500\text{-}800\text{ cm}^{-1}$ and $1100\text{-}1700\text{ cm}^{-1}$. The strongest peaks are at 670 , 770 , 800 , 1240 , 1480 and 1570 cm^{-1} . The sugar backbone gives rise to weak bands from 800 to 1100 cm^{-1} as well as contributions to the strong CH_2 deformation peak around 1460 cm^{-1} .

3.1.3 Lipids

Cellular and subcellular organelles are surrounded by membranes, which are built up of a bilayer of phospholipids. The Raman spectra of phospholipids contain vibration modes both from the hydrophilic head and the hydrophobic hydrocarbon tail. The C-N vibration in the polar head of the phospholipid gives rise to a 720 cm^{-1} peak and the hydrocarbon chain exhibits C-C skeletal vibrations between 1000 and 1150 cm^{-1} which are sensitive to membrane conformation.

3.1.4 Differences in Raman signals from normal and malignant tissue

A Raman spectrum contains numerous peaks originating from tissue compounds that are present in all types of tissues. The individual peaks are easily identified with known molecular vibration modes; however, the interpretation of the peaks in molecular constituent concentrations and the subsequent interpretation to malignant or healthy tissue requires a rather complete understanding of the molecular, microscopical and macroscopical origin of observed Raman peaks. Results from measurements of Raman spectra *in vitro* from different tissue types suggest that Raman spectroscopy is a powerful method^{27,28}. However, the question whether information from peak intensities and positions can be converted to consistent and robust diagnostic criteria, useful for *in vivo* studies, still has to be answered³⁰. Work along these lines has been performed to determine the molecular concentration of human artery material³¹⁻³⁴ and to determine the molecular concentrations as a function of tissue depth in normal skin³⁵. Raman spectroscopy has also been shown useful for the measurement of concentrations of multiple analytes in human serum³⁶ and in whole blood³⁷ and to qualitatively analyse the cholesterol and cholesterol esters in atherosclerotic plaques³⁸.

Differences in Raman spectra recorded from various benign and malignant skin lesions have been reported^{39,40} and *in vitro* studies have shown success of discriminating basal cell carcinoma from normal skin^{41,42}. The ability of Raman spectroscopy to correctly classify normal breast tissue samples and benign and malignant breast tumours has been shown⁴³. The spectral differences in normal and diseased breast tissues have been attributed to the fact that normal tissue is mostly composed of lipids and proteins and diseased tissue is composed of proteins.

In a survey conducted in 1996 by Manoharan *et al.*²⁷, the usefulness of near-IR Raman spectroscopy for characterizing malignant tissue in the colon, urinary bladder, breast and other soft tissue carcinomas is questioned. The results suggest, that Raman spectroscopy is less useful for probing cancerous alteration restricted to the epithelial surface. This is due to the fact, that Raman spectroscopy is a less sensitive method than fluorescence or absorption, even though it provides much more information, and

that the penetration depth is in the order of 1 mm. Early changes in epithelial tissues are very shallow and the Raman spectra can be completely dominated by the signal from underlying normal tissue.

However, promising results of epithelial changes have been recorded from studies using Raman spectroscopy in the detection of cervical pre-cancers⁴⁴ and for the investigation of various gastrointestinal tissue types⁴⁵.

Within the present thesis (Paper I), clinical application of Raman spectroscopy has been performed and is discussed more in detail below.

3.1.5 *In vitro* versus *in vivo* studies

Many Raman spectroscopy studies on tissue have been performed *in vitro*. Normally, fresh tissue samples are snap frozen and stored in liquid nitrogen or deep frozen at -80°C. The tissue is thawed in room temperature before measurements and is kept moist with phosphate buffered saline. This method has been proven not to induce any artifacts in the Raman spectra⁴⁶.

3.2 Instrumentation and evaluation

The Raman signal from tissue is extremely weak. Therefore many groups have used a Nd:YAG laser at 1064 nm and a Fourier-Transform (FT) spectrometer to obtain Raman spectra in the infrared region, where the fluorescence is almost completely suppressed. However, these early systems required long data collection times of 3 to 30 minutes⁴⁷⁻⁴⁹ and were not compatible with fibre optics. The signal-to-noise ratio was limited due to the reduced scattering cross section at 1064 nm and the large noise in the detectors in the range 1100 to 1350 cm^{-1} . When the CCD detectors sensitive in the NIR region were developed, the first systems employing a NIR excitation and a CCD detector were built by different groups^{44,50-52}. These systems were developed and are now capable of collecting a Raman spectrum in a few seconds using fibre optical probes^{45,53-55}.

3.2.1 Excitation wavelength

NIR excitation is chosen as it reduces the fluorescence background and noise in Raman spectra. The proper excitation wavelength has to be chosen by balancing the fluorescence reduction for a longer wavelength with the quantum efficiency drop for the detector at longer wavelengths. In reality this means that systems with excitation wavelengths between 700 to 850 nm are preferred. It should be noted that it is mainly the shot noise level from fluorescence that has to be reduced; the baseline from fluorescence can be subtracted by different techniques. This is clearly illustrated in a study where the Raman spectra from breast samples were measured using several different excitation wavelengths in the range 406 to 830 nm⁵⁶. The ratio of Raman signal to fluorescence intensity is higher for 830 nm. Actually, the spectra reported from the group in Rotterdam³⁵ using 850 nm excitation do not show any large fluorescence background compared to spectra recorded with similar equipment using excitation wavelength at 785 nm (Paper I, Ref.⁴⁵).

An alternative way of reducing tissue fluorescence is to employ UV excitation at wavelengths below 270 nm, which can match electronic energy states. In biological materials, the high-lying electronic states excited by UV light often rapidly relax via non-radiative process to lower-lying levels, thereby eliminating fluorescence or causing it to occur at much longer wavelengths. Raman-scattered light is generated before the relaxation process and is emitted in the UV region. The method is called UV resonance Raman (UVRR) spectroscopy and has been used for studies of biological material⁵⁷. However, UV light can induce mutagenesis and the tissue penetration depth is small leading to small probe volume. The method can be used *in vitro* but it is not a candidate for *in vivo* tissue characterization.

The use of a near-infrared excitation wavelength leads to a fairly large penetration depth and thus a relatively large probe volume. For 785 nm excitation, the reduced scattering is approximately $\mu'_s = 11 \text{ cm}^{-1}$ for skin⁵⁸. The effective penetration depth is estimated to 3-4 mm. Thus, the probe volume of Raman spectroscopy is large compared to other spectroscopy methods like, for instance, fluorescence spectroscopy.

3.2.2 Temperature considerations

Since the Raman signal is inherently weak, quite high powers of laser irradiation are needed (~100-300 mW). Fibre probes are used for *in vivo* and *in vitro* Raman spectroscopy and focused beams are used in *in vitro* set-ups. Large power densities are created at the tissue surface, which leads to heat generation and there is a possibility that the heat can induce tissue damage and/or alter the Raman signal. Shim *et al.*⁴⁶ examined the effects of tissue heating *in vitro* with a focused beam (wavelength 1064 nm, power 450 mW, 0.5 mm diameter, 30 min illumination) with the result of no alterations in the Raman signal and no visible damage, but there have been very few other examinations with other parameters. It would be interesting to perform the same study for wavelengths in the range 750-850 nm.

3.2.3 Spectrographs

The choice of the spectrograph is also important. The spectrograph should have a high numerical aperture and be compatible with an imaging CCD detector. Dispersive spectrographs with a holographic grating have a large throughput, compact design, reasonably flat image field and can easily be matched to a fibre. Sharp holographic notch filters are used in the spectrograph to suppress the strong Rayleigh scattered excitation light entering the spectrograph. The optical layout of a typical system (HoloSpec f/1.8i-NIR, Kaiser Optical Systems Inc., Ann Arbor, MI) is shown in Fig. 7.

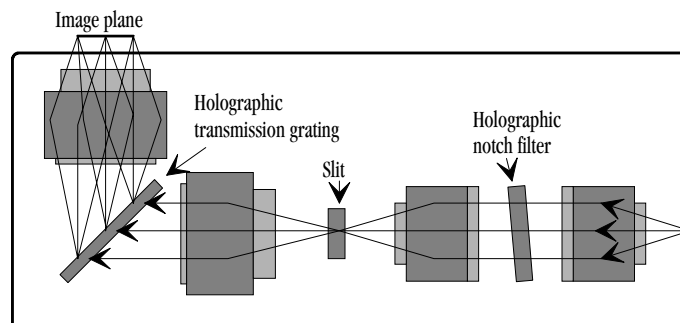


Figure 7. Optical layout of HoloSpec f/1.8i.

3.2.4 Detectors

An appropriate CCD detector has to be chosen. Back-thinned CCD detectors have higher quantum efficiencies than front-illuminated ones. However, a fixed sensitivity pattern can be introduced, since the thin silicon wafer acts like an etalon. In addition, by using a deep-depletion CCD, one obtains an increased quantum efficiency in the NIR region. The detectors are cooled to reduce the noise. Liquid nitrogen has been and still is used for cooling. However, during the last few years, CCD detector technology has improved and it is now possible to use Peltier cooling without much detector noise.

The choice of detector temperature is a trade-off between low detector noise and high quantum efficiency, since the quantum efficiency is slightly higher at higher temperatures. For the detector we have been using for Raman spectroscopy (LN/CCD 1024 EHRB, Princeton Instruments Inc., Ontario, Canada), the optimal detector temperature should be between -70°C and -90°C ⁵⁹.

3.2.5 Optical fibre probes

For most medical application, fibre probes guiding excitation and Raman scattered light are needed to be able to measure on remote internal organs inside the body through endoscopes, needles and other clinical devices. To be able to comply with safety precautions, the instrumentation should be situated away from the patient; thus the fibre has to be several meters long. An optical fibre probe should also be compatible with standard sterilisation procedures. It is not trivial to fulfil these specifications of fibre probes for Raman spectroscopy.

Fibre transmission in the NIR region is quite good using special low-OH quartz fibres. However, the main problem with fibres is the strong silica Raman scattering signal. This is generated both in the fibre transmitting the excitation light to the tissue and in the collection fibre, where scattered excitation light enters the fibre and generates Raman scattered light on the way to the spectrometer. In fibres of several metres, the fibre Raman signal can be much stronger than the tissue Raman signal.

To solve the problem, optical filters are needed. These must be positioned at the distal end of the fibre probe, actually in the tip of the fibre. One narrow-banded filter is needed in the excitation fibre to clean the output from fibre emission. In front of the collection fibre, a sharp notch filter or cut-on filter, blocking the scattered excitation light is necessary. The filters are small and have to be manufactured in a quartz substrate. Many groups have developed their own Raman probes for various clinical applications^{51,55,60}.

There are commercial fibre probes available. The Enviva Biomedical Raman probe (Visionex Inc., Atlanta, GA, USA) has been used *in vivo* for Raman spectroscopy of gastrointestinal tissue⁴⁵ and to determine the molecular composition of the artery wall³⁴. The probe consists of one 400 μm emission fibre surrounded by seven 300 μm collection fibres. This probe utilises beam-steering (Gaser Fiber Optic Light Management Technology, Visionex Inc., Atlanta, GA, USA), which improves the overlapping region between emission and collection volumes in the probe; see Fig. 8. Further, the internally incorporated filters in the probe tip reduce the influence from silica fibre Raman and fluorescence emission significantly and improve the performance of the fibre probe⁶⁰. Unfortunately the probe is not compatible with autoclavation and has to be sterilized by soaking in glutaraldehyde, which is toxic.

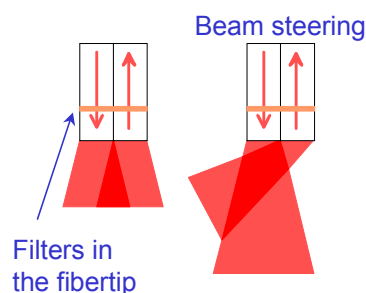


Figure 8. The left picture illustrates the normal overlap between excitation light and collection geometry. To the right, the beam-steering and internal filters in the Visionex probe for Raman spectroscopy are shown.

3.2.6 Background subtraction

The fluorescence from tissue is much stronger than the Raman signal and contributes a lot to the noise in the spectra. There are a number of different spectroscopy techniques and post-recording computer analysis techniques that can suppress the fluorescence background. These are all based on the differences in the scattering process of Raman and fluorescence.

The fluorescence background is normally broad and the Raman peaks are sharp and thus the background can potentially be eliminated from recorded spectra by the use of shifted spectra techniques and edge detection⁶¹. Another technique is to Fourier transform the spectrum, apply a high pass filter removing the lowest frequencies and then apply the inverse transform. Perhaps, the most common method is to subtract a low-order polynomial fitted to the raw spectrum. The result is a Raman spectrum with both negative and positive values.

The fluorescence rejection method employed in Paper I was developed during a Master Thesis project in co-operation with the Department of Mathematical Statistics⁶². A non-parametric Kernel regression technique was developed to filter the spectra obtained. The original spectrum $Y(x)$ is modelled as $Y(x) = m(x) + \sigma(x)\varepsilon(x)$, where $m(x)$ is the signal without noise, $\sigma(x)$ is the standard deviation of $Y(x)$ and $\varepsilon(x)$ is white noise. $m(x)$ is the sum of the fluorescence signal, $m(x)_F$, and the Raman signal $m(x)_R$. The procedure can be seen in Fig. 9. $m(x)$ is estimated by non-parametric Kernel regression with local bandwidths. $m(x)_F$ is estimated by non-parametric Kernel regression with a large and global bandwidth. The Raman signal $m(x)_R$ is then estimated as $m(x)_R = m(x) - m(x)_F$. The method shows good fluorescence background rejection.

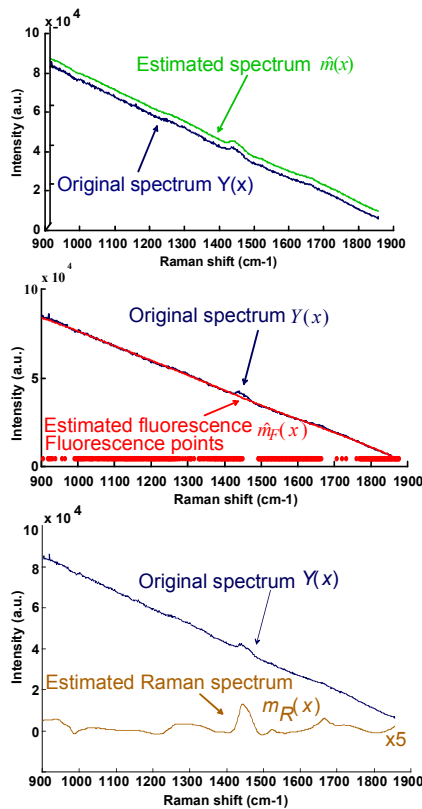


Figure 9. The Kernel regression method is illustrated for a Raman spectrum.

3.2.7 Multivariate methods

A Raman spectrum contains a vast number of peaks, which represent vibration modes present in many different molecules. The relative intensity between different peaks and the absolute vibration frequency are clues to which molecules are present and in which environment. In order to build a model for characterization and classification of tissue,

multivariate methods are required due to the complex problem.

The multivariate methods of Principal Component Analysis (PCA) and Partial Least Squares (PLS) are commonly used methods. These methods were first employed in chemical analysis and are often referred to as Chemometrics.

Often the principal components or the partial least squares components are used as input to some classification algorithm. In cases, where the spectra from the suspected constituents in the sample are known, a hybrid linear analysis using the PLS components from the training set and the spectra from the species of interest can give a more precise prediction than the pure PLS prediction⁶³. The use of neural networks is a different approach, which in some cases have proven to be successful⁴¹.

In the development of methods for concentration analysis and tissue discrimination, two sets of data are needed. The first set is a calibration set, where spectra taken from known compositions or diagnoses are used to build the model. Then, an independent test set is required to determine the prediction ability of the model. Also here the composition or diagnosis has to be known. These sets require a large quantity of data and a way to use a single set is to apply cross-validation. In this method, one spectrum is left out and tested using the model built on the remaining spectra. Then the procedure continues by removing the next spectrum, etc.

3.3 *Clinical applications*

Raman spectroscopy probes the biochemical composition of a biological material and is thus a potentially useful method for non-invasively biomolecular detection of tissue malignancies and other changes. In this section, applications in the cardiovascular and skin are discussed. However, Raman spectroscopy also has applications in breast cancer detection^{43,56}, measurements of analytes in human serum³⁶ and whole blood³⁷, brain tissue⁶⁴ and for the detection of cervical lesions⁴⁴.

3.3.1 **Cardiovascular applications**

There has been an intense interest to use NIR Raman spectroscopy to gain information concerning the biomolecular changes with the progression of atherosclerosis. Several studies have been conducted *in vitro*^{25,31-33,38,47,65,66}, and *in vivo* work in an animal model has also been performed³⁴.

During early atherosclerosis the intima thickens due to smooth muscle cell proliferation and migration into the intima of the vessel, and collagen accumulation. Elastin breakdown, lipoprotein accumulation and calcification follow. The build-up of necrotic material and crystallisation of calcium apatite lead to complex bulky atheromas, which can result in major complications. Lipids, mostly cholesterol and cholesterol esters, account for roughly 60% of the dry weight of the intimal layer of an atheromatous plaque. Raman spectroscopy may be able to measure all these constituents and provide the clinician with information for evaluating the type and degree of severity of the disease, which is needed to initiate the proper treatment strategy.

Studies of minced and intact arteries showed that it is possible to build a model of Raman spectra and determine the composition of the sample^{31,32}. Using an animal model, this method has been used *in vivo*, and detailed information about the chemical composition of the blood vessel wall can be obtained³⁴.

The first Raman spectroscopy study on vessels was performed by Clarke *et al.*²⁵ using visible excitation at 514.5 nm. Raman peaks could be observed, but the intense fluorescence produced significant interference.

During the years 1997-1999, the Lund group was involved in a joint European collaboration project program called Laser Assisted Investigations in Cardiology (LAIC). The aim was to evaluate the potential of optical methods for the characterization of cardiovascular tissue. Fluorescence, reflectance and Raman spectroscopy systems were constructed and used in clinical campaigns. In 1997, *in vitro* Raman measurements of cardiovascular tissue samples were performed in London, and in 1999 *in vivo* measurements of cardiovascular tissues were performed during open heart surgery and surgery of peripheral vessels.

The equipment used has been discussed previously in this thesis and the set up for clinical measurements can be seen in Fig. 10. The emission from a tuneable diode laser emitting at 785 nm was coupled into an Enviva Raman probe. The laser emission out from the probe was about 15-55 mW. The Raman scattered light was transported through the probe into the spectrometer and captured by a nitrogen cooled CCD detector. The integration time for the *in vivo* measurements was 10 s. A picture from the measurements can be seen in Fig. 11.

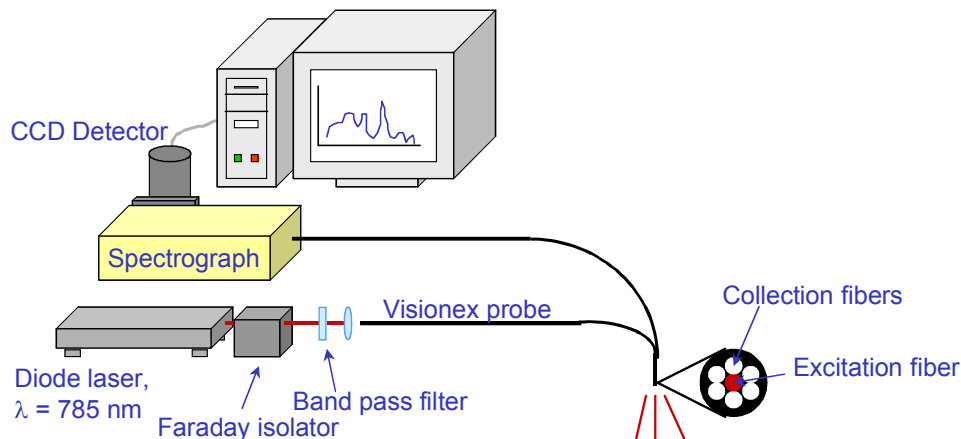


Figure 10. The setup for clinical measurements.



Figure 11. *In vivo* Raman spectroscopy measurements during open heart surgery. The author of this thesis is filling out the protocol in the back.

Measurements were performed on 11 patients. A representative spectrum recorded from the inside of an abnormal femoral artery can be seen in Fig. 12.

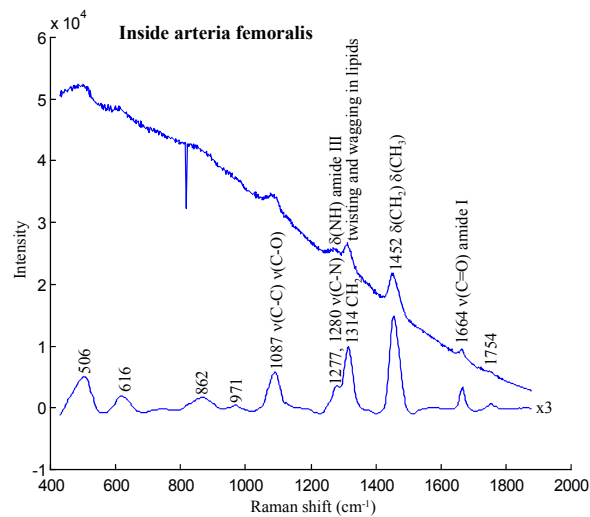


Figure 12. Raman spectrum recorded from the inside of the arteria femoralis. The top curve represents the raw data and the lower curve is the filtered signal.

Many of the observed peaks can be identified as seen in the figure.

Comparing several spectra did not provide any clear indication of any distinct differences between spectra recorded from various tissue types. The spectra show indeed Raman peaks. However, the fluorescence background is high and small low intensity peaks cannot be resolved. These results were presented at a conference in 1999⁶⁷ but have not been published elsewhere, due to the relatively low number of patients and recorded spectra.

3.3.2 Oncological dermatology

The skin is a complicated organ, which comprises different layers, all with different morphology and molecular composition. Outermost, the dead horny layer of stratum corneum forms an important barrier. Below this is the epidermis, which is a thin layer primarily consisting of keratinocytes, which are cells that prevent the entry of toxic substances from the environment and the loss of important constituents from the body, mainly by the tight intercellular adhesion. The dermis is a thicker layer, which is largely composed of collagens. Hair roots, glands, nerves and a vast network of capillaries are located within the dermis.

There has been some interest to use Raman spectroscopy for the characterization and classification of skin lesions. NIR-FT Raman spectroscopy has been used for the characterization of normal and diseased skin^{40,68}. In the studies by Caspers *et al.*^{35,52}, the qualitatively variations of composition of different skin layers could be measured *in vivo* in a straightforward non-invasive rapid manner. The molecular abnormalities in benign and malignant skin lesions have also been investigated^{39,41}. The same group has also used Raman spectroscopy for the investigation of protein structure in aged skin⁶⁹, the structure of water, protein and lipids in human skin⁷⁰ and investigation of mummified skin⁷¹.

In Paper I, an *in vivo* study of skin lesions is presented. For this work, our Raman system was modified into a mobile clinical system. The equipment was put on a trolley covered by a light proof hood; see Fig. 13. In this way, clinical recordings could be performed without any fibre optic probe, even if the patients had to position themselves into awkward positions in front of the 3 centimetres wide opening, where the measurements were performed. The skin surface was illuminated from the inside with a white-light halogen lamp. A small RGB camera recorded the skin for easy visual alignment and a 600 μm quartz fibre collected reflected light to record the reflection spectra from the centre position of the skin in the opening; see Fig. 14.

Even if the recorded spectra clearly exhibited several Raman peaks, subsequent multivariate analysis showed that there is not any diagnostic information in these strong peaks (Paper I). Minute differences in molecular composition between normal and malignant tissue might not influence the strongest peaks, which are present in all tissue types. These conclusions put high demands of a clinical system to be able to produce high resolution, low-noise Raman spectra in a few seconds.



Figure 13. Raman setup.

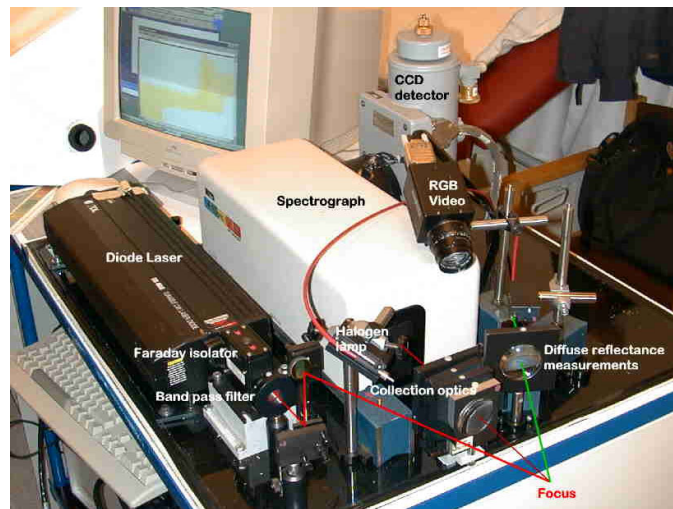


Figure 14. Optical layout.

4 Fluorescence spectroscopy for tissue characterization

Fluorescence spectroscopy is a method with potential to non-invasively characterise different tissue types and to classify tissue. Of special importance is the ability to delineate the borders between normal and malignant tissue and to guide biopsy sampling to the most likely diseased tissue section during the clinical examination. Especially in those clinical specialities, where malignant tissue cannot be visualised easily by the eye and random sampling can be necessary, fluorescence guiding is valuable.

The instrumentation for fluorescence spectroscopy is relatively simple compared to Raman spectroscopy, since the fluorescence signal from tissue is much stronger. However, to be able to measure in a clinical environment, optical fibre probes are required for easy access through endoscopes or needles, and time-gated detection is often required for the elimination of ambient light. In addition, a clinical system should be small for easy transportation and use.

The information from a fluorescence spectrum can be difficult to interpret since the fluorescence emission is dominated by a few fluorophores with broad and overlapping spectra. Mathematical multivariate tools are often required to separate the fluorescence from different fluorophores and to build models for tissue classification. A thorough review of different methods for analysis of fluorescence spectra can be found in Ref.⁴.

The use of externally applied fluorescent tumour-seeking sensitizers can enhance the discrimination substantially. Further, different fluorophores have different absorption maxima and fluorescence instruments utilising multiple excitation wavelengths may provide additional information.

Clinical fluorescence spectroscopy of tissue was introduced as a diagnostic tool for malignant lesions by Profio *et al.*⁷² in the 80:s and since then, several studies have been conducted pertaining to many various clinical applications.

4.1 Autofluorescence

Tissue that is illuminated with light in the UV/blue spectral range normally fluoresces in the blue-green region of the visible spectrum. This is called the autofluorescence or the endogenous fluorescence and originates from a number of fluorescent proteins, flavins and porphyrins. These fluorophores all have individual absorption and emission maxima; see Table 1.

The emission spectra from these compounds are normally broad due to the large number of vibrational levels and the interaction between neighbouring molecules. The fluorescence spectra from some of the most abundant fluorophores can be seen in Fig. 15.

Fluorophore	λ_{exc} (nm)	λ_{em} (nm)
Tryptophan	275	350
Collagen	340	395
	270	395
	285	310
Elastin	460	520
	360	410
	425	490
	260	410
NADH	350	460
β -karoten		520
Endogenous porphyrins	400	610, 675

Table 1. Wavelengths for excitation and emission maxima for the most abundant fluorophores in tissue. Taken from Ref.⁷⁵.

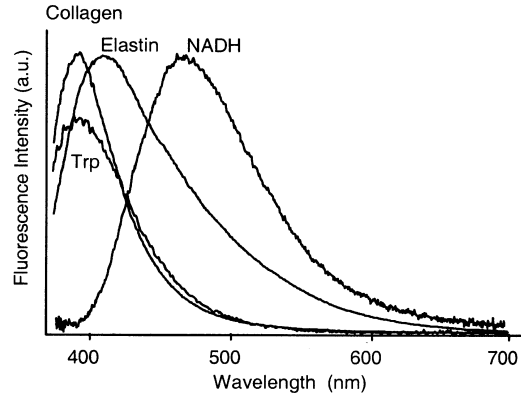


Figure 15. Fluorescence emission from some tissue fluorophores, excited at 337 nm. Adopted from Refs^{73,74}.

4.1.1 Collagen

Collagen is a strongly fluorescent protein that is abundant in connective tissue. There are several different types of collagen which have slightly different absorption and emission characteristics. Collagen I is the most abundant type and it forms long fibrils. It can be found in the connective tissue in the skin and in tendon, bone and dentin. Collagen IV forms sheets and can be found in the basal membrane of epithelial tissues.

4.1.2 Elastin

Elastin is another protein, which is the major part of elastic fibres. These elastic fibres impart extensible and resilient character to tissues such as the dermis, lung and large blood vessels.

4.1.3 NADH/NAD⁺

Nicotinamide adenine dinucleotide (NADH) is the reduced (electron-energy rich) coenzyme form of vitamin B₃, while NAD⁺ is the oxidized (burned) form. NAD⁺ and NADH are converted into each other in numerous different metabolic activities and carry the energy in the electron transport chain, where much of the ATP bioenergy, that runs every biological process of our body, is formed. NADH/NAD⁺ is most abundant in the respiratory unit of the cell, the mitochondria, but is also present in the cytoplasm.

In tumours, where an intense oxygen-consuming metabolism is present, the oxygen level might be lower, leading to a reduced pH-value that will influence the redox balance between NADH/NAD⁺ concentrations. NADH is highly fluorescent while NAD⁺ is not seen when the tissue is excited above 300 nm. If the equilibrium is pushed towards a lower concentration of NADH, this might lower the blue-green fluorescence originating from NADH. The blue-green autofluorescence from malignant and pre-malignant lesions has been reported lower than in healthy tissue in many *in vivo* studies⁷⁶⁻⁸⁰.

4.1.4 Other fluorophores

Tryptophan is an essential amino acid, which is the precursor of one of the most important antidepressant neurotransmitters, serotonin. Tryptophan is a strong fluorophore for excitation wavelengths below 300 nm and it might be a useful discriminator, since strong fluorescent levels have been seen in cervical epithelial cancer cells⁸¹. Other endogenous fluorophores include flavins^{82,83}, lipofuscin⁸⁴, β -carotene⁷⁷ and porphyrins^{85,86}.

4.1.5 Absorbers

The presence of absorbers like haemoglobin and melanin drastically alters the recorded fluorescence spectrum from tissue. These absorb the excitation wavelength and can thus drastically lower the over-all intensity of a recorded spectrum. The haemoglobin absorption spectrum is shown in Fig. 5. Oxygenated (HbO₂) and deoxygenated haemoglobin (Hb) have different absorption spectra. The strongest absorption peaks can be found at 414, 542 and 577 nm for (HbO₂) and at 433 and 556 nm for Hb.

The generated tissue fluorescence emission is absorbed by haemoglobin and thus 'artificial' peaks and valleys are created in the resulting fluorescence spectrum. One way to evaluate fluorescence spectra is to calculate intensity ratios at wavelengths with equal haemoglobin absorption⁸⁷ as also used in the double ratio technique⁸⁸ or to use a reflectance spectrum to estimate the concentration of haemoglobin and eliminate the blood interference⁸⁹.

4.2 Fluorescent tumour markers

Autofluorescence gives a possibility to probe the tissue constituents. In order to increase the sensitivity of demarkating malignant from normal tissue, fluorescent tumour-seeking markers are widely used. These are ring-structured molecules that are to a certain degree selectively accumulated in malignant or pre-cancerous tissue after administration topically, intravenously or orally. The markers exhibit fluorescence emission in the red or near infrared wavelength region and can thus be easily distinguished from the blue-green autofluorescence. The same substances are often used as photosensitizers for selective treatment of malignant tumours, photodynamic therapy (PDT), but then administered in higher concentrations as compared to diagnostic use. PDT is discussed in the next chapter.

Many various markers can be used for fluorescence induction and PDT, and an overview can be found in the thesis by af Klinteberg⁹⁰. The marker used in the present thesis (Papers V, IX-XIV) is 5-aminolevulinic acid (ALA) induced-protoporphyrin IX (PpIX), which is perhaps currently the most used and popular fluorescent tumour marker.

PpIX is produced in the haem biosynthetic pathway after the access administration of 5-aminolevulinic acid (ALA). ALA is endogeneous amino acid, which is required for the synthesis of haemoglobin. Protoporphyrin is the last molecule in the haem cycle before incorporation of the Fe iron by the action of the enzyme ferrochelatase; see Fig. 16. The normal production of PpIX is regulated by a feedback mechanism. However, if ALA is given in excess amounts, PpIX will build up temporarily during a couple of hours. It has been shown that in some premalignant and malignant tissue, the ferrochelatase activity is reduced, while the activity of the porphobilinogen deaminase is enhanced^{92,93}. This enzymatic difference leads to that PpIX is built up in a higher degree in diseased cells as compared to in normal cells.

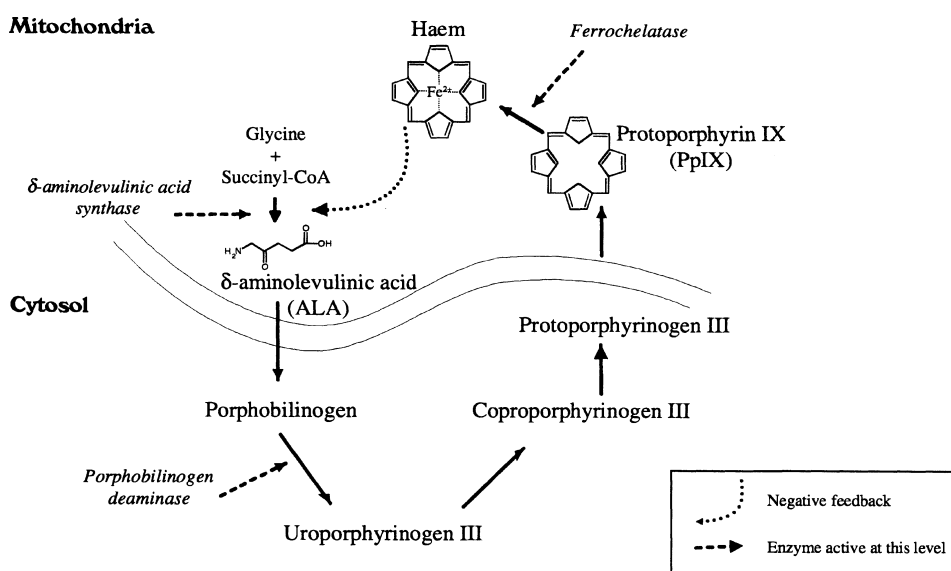


Figure 16. Biosynthetic pathway of haem. Adapted from Ref.⁹¹.

The kinetics of PpIX build up varies with location and the administration route of ALA. For oncological dermatological application, ALA is normally mixed into a creme and applied topically. Actually, the selectivity of ALA uptake in skin lesions is mainly due to the increased permeability of a skin lesion. For most other applications, ALA is given orally, diluted in juice. In brain tumours, the selectivity is believed to mainly be caused by the damaged blood-brain barrier.

PpIX has its absorption maximum at 405 nm and fluoresces with two peaks in the red region, 635 and 700 nm. After administration of ALA, the maximal PpIX fluorescence emission is seen after 4-6 hours in skin malignancies⁹⁴ and most of the PpIX is cleared within a few days or even faster.

4.3 Instrumentation and evaluation

Fluorescence spectroscopy is technically rather easy to implement in a system due to the fact that the fluorescence emission is quite strong. However, to build a useful system requires the fulfilment of many specifications. First of all, the excitation wavelength has to be matched to the absorption of the compounds of interest. For autofluorescence, this means an excitation at low wavelengths like the N₂ laser at 337 nm. The absorption band of the commonly used fluorescent tumour markers is often around 400 nm (405 nm for PpIX), which implies that there should be a possibility of two excitation wavelengths for optimal results. Further, if the light source is pulsed with short pulses, the use of gated detection makes it possible to measure in a clinical environment without disturbance from ambient light. Optical fibres make the system accessible to all endoscopic sites. Such systems have successfully been built by many research groups⁹⁵⁻⁹⁷, including the group in Lund^{98,99}, but there is still no point-monitoring commercially available system. Fluorescence imaging systems have also been built by different research groups¹⁰⁰⁻¹⁰⁶ and there are several commercial systems available or under development (HyperSpectral Diagnostic Imaging[®], Science and Technology Int., Honolulu, HI, USA; Cerviscan[™], LifeSpex Inc., Bothell, WA, USA; LIFE, Xillix Technologies Corp, Richmond, BC, Canada; D-Light/AF system, Karl Storz, Tuttlingen, Germany). However, the implementation of an automatic real-time evaluation algorithm is a crucial step towards the acceptance and use in the clinic. Some systems provide the fluorescence image to be interpreted by the clinician, and others use complicated algorithms for the delineation of tumour areas and borders. A recent review is provided in Ref.¹⁰⁷.

4.3.1 Diode fluorosensor

The development of blue diode lasers and compact spectrometers provide a possibility to manufacture small and inexpensive systems, which is important for clinical applications. One such system was constructed and is presented in Paper IV.

The diode fluorosensor is capable to monitor the fluorescence with spectral resolution enough for evaluation. The measurements can be performed using optical fibres and the accumulation time is only a few seconds. However, the system does not provide gated detection, which makes it very sensitive to ambient light. This problem can to some extent be overcome by measuring the ambient light passing through the tissue with the fibre in contact and then subtract this background from the recorded fluorescence spectrum. This technique has been used in the software especially written for this system¹⁰⁸. The fluorescence from the optical fibre is measured in darkness and it is also subtracted.

At the time when the system was built, the shortest wavelength available for blue diode lasers was 396 nm. This wavelength suits PpIX excitation, but it is perhaps too long to be able to do discrimination using autofluorescence. Mostly NADH is excited at 396 nm but no information from i.e. collagen and elastin is gained.

4.3.2 Spectral evaluation methods

In order to have optical systems that in real-time can analyse and discriminate pre-malignant or malignant tissue from healthy tissue using the complex information from recorded spectra, statistical models have to be implemented. By different methods, the fluorescence (or Raman) spectra have to be evaluated and the information be reduced to a value that can provide tissue characterization. Tissue consists of a few major fluorescent molecular species and in addition, other absorbing non-fluorescent substances and scattering influence the recorded spectrum. The variation in intensity between individual patients is considerable and some kind of normalisation is often needed. This is commonly done by area normalisation.

The evaluation methods used in this thesis are, as already discussed in Sect. 3.2.7., mainly Principal Component Analysis (PCA) and Partial Least Squares (PLS). To use these methods, all spectra are stored in a matrix X . PCA is the same as single value decomposition to find the eigenvalues (scores) and eigenvectors (principal components) in the matrix X . Unless the spectra are normalised, the first principal component, PC 1, will be the average spectrum of all spectra in the matrix and the score for the first component will reflect the general intensity in the fluorescence spectra. The information from the first component is then subtracted from the original matrix and the single value decomposition is performed again to calculate the second component. The second principal component will be a spectrum representing the most common deviations from the average spectra. For fluorescence spectra, the first few components contain useful information, and higher component just represent noise. In this way, the information from a full spectrum can be reduced to a few scores.

To be able to correlate spectra to tissue types, a large set of spectra together with the corresponding pathology are needed. The set is divided and one part is used to build a model in which the other spectra are tested. Using PLS, the principal components are calculated with the influence of the known pathology to create the component, which corresponds to the variation in the pathology vector. In the prediction procedure, the root mean square error of prediction (RMSEP) is the parameter used to determine the number of components to be used in the model. A PLS model for prediction was used in Papers I and III.

4.4 Clinical applications

In this thesis several studies have been performed *in vitro* and *in vivo* for various clinical purposes. Tissue composition and morphology are clearly different for various applications and a brief summary is given below for the applications suggested in this thesis.

4.4.1 Cardiovascular

The aim in cardiovascular applications is the identification and molecular analysis of atherosclerotic plaques, dose adjustment of immunosuppressive medications to prevent rejection of transplanted organs as well as localisation of subendocardial ischemic or infarcted myocardium. Measurements of *in vivo* fluorescence spectra were performed on two occasions within the LAIC project. In total, fluorescence spectra from 24 patients were recorded on various tissues during cardiovascular surgery and heart transplantation. Both healthy and abnormal vessels were measured and spectra were recorded from the outside and the inside. The epicardium (outside) of the heart was measured as well as vessel malformations. In Fig. 17, spectra measured from one patient with an aneurysm are shown.

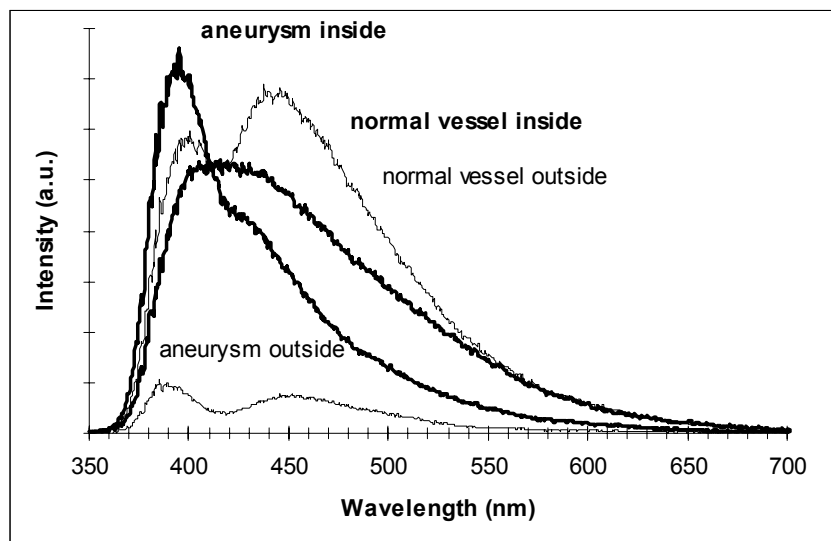


Figure 17. Fluorescence spectra recorded *in vivo* on the outside and inside of a normal peripheral vessel and an aneurysm.

PCA and PLS were performed on all spectra to identify spectral shapes corresponding to tissue morphology. The total number of fluorescence spectra recorded was quite large; however, after separating into homogeneous groups, the numbers are too low to evaluate statistical findings.

In Paper III, measurements on endocardial biopsies are described. The results showed that fibrous tissue could be distinguished from normal endocardium. The real interesting question if inflammation (a sign of heart tissue rejection) could be detected, remains unsolved due to the few cases of inflammation obtained in the study.

4.4.2 Skin

Fluorescence spectroscopy can be used to discriminate the border between malignant skin lesion and healthy skin. The autofluorescence is normally significantly lower in the lesions and the detection is further enhanced with the use of a fluorescent tumour marker. In some types of skin lesions, for instance in basal cell carcinoma (BCC), the border is not always easy to distinguish with the naked eye.

4.4.3 Cervix

The uterine cervix is biologically complex and the transformation zone is a very active area. To help the understanding of Papers VI-VIII, the morphology is shown in Fig. 18. The vagina is covered with squamous epithelium and the inner lining of uterus consists of columnar epithelium reaching out through the cervical channel to the cervical area. The columnar epithelium is transformed to squamous tissue and this region with intense cellular activation is called the transformation zone. The exact position of the border varies with the menstrual cycle and with age. The cervical lesions are to more than 90% formed in this region.

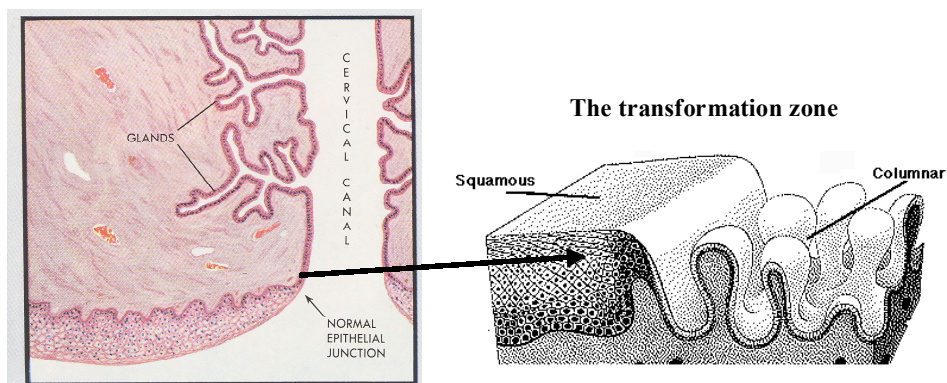


Figure 18. In the left micrograph, thin, columnar epithelium lining the inside of the cervical channel is shown and it is transformed to thick squamous epithelium, which covers the cervical area. In the schematic picture to the right, this transformation zone is shown.

4.4.4 Brain

Malignant tumours in the brain have in general two different origins. Some of them are metastases from tumours somewhere else in the body. The primary brain tumours, which are developed from the glia cells in the brain, are more or less impossible to remove radically during surgery due to the infiltrating growth pattern. The discrimination between tumour and normal brain tissue is guided by changes in texture, consistence and colour, but no distinct border is usually seen.

Fluorescence spectroscopy could possibly provide a method for tissue characterization in this clinical situation and the vision is that an optical fibre probe could be inserted into the sucker used for tumour excision. The removal would then be guided by real-time analysis of recorded fluorescence spectra. The autofluorescence of normal and tumour tissue is similar but by the use of a fluorescent tumour marker, the tumour seems to be clearly visualised. This has been examined in Paper V, and the results are promising; however, the statistical significance is low.

The accumulation of PpIX in the brain is not related to the metabolism; rather to the damaged blood-brain barrier in tumours that allows ALA to leak in. However, there is a non-trivial source of error due to the leakage of ALA to surrounding healthy tissue.

5 Photodynamic therapy

The first photodynamic therapy (PDT) procedures utilising hematoporphyrin derivatives (HpD) were performed during the early 1960:s. The field of research in PDT has since then expanded. Today PDT is an approved method in several clinical situations and there are commercial laser systems and drugs available. The main advantages of PDT are the selectivity, the nice healing and the ability to retreat the same area many times, if necessary. The main disadvantage of PDT is the limited light penetration, which on the other hand can be improved by development of photosensitizers active in the NIR wavelength range, and using the concept of interstitial PDT.

In this chapter the most basic principles of PDT are described together with some of the biological treatment-related mechanisms investigated in Paper X. A more thorough description of photosensitizers, technical instruments, the treatment mechanisms of PDT and clinical applications is given in for instance Refs^{90,91}. An introduction to the concept of photodynamic threshold dose is given below and an estimation of the photodynamic threshold for PpIX is presented in Paper XII.

5.1 Principles of action

Basically, the treatment effect from PDT relies on the presence of three reactants, sensitizer, light and oxygen, all in the proper location and quantity. The photochemical reaction between these constituents causes crucial damage to the tissue and leads to tumour cell necrosis, apoptosis, vascular damage and secondary inflammatory reactions.

PDT has some advantages compared with other tumour treatment modalities (radiation, excision, cryotherapy). Since the sensitizer accumulation is selective to a certain degree, healthy tissue can be illuminated at low risk and full treatment can be given to the tissue just outside the visible tumour margin, where there is a probability that non-visual pre-cancerous cells are present. Further, the healing is fast and there is almost no scar formation. If the response of the treatment is only partial, the treatment can be repeated an unlimited number of times, since there is no memory in the tissue of the treatment, as in the case of conventional radiation therapy. The procedure is relatively easy to perform, does not require too much expensive equipment, and if laser goggles are worn during the whole procedure, there are few potential hazards. Patients experience pain in various degrees; however, generally no anaesthesia is required.

As mentioned above, the main disadvantage of PDT is the limited light penetration depth, limiting the treatment to superficial tumours. With the development of photosensitizers active in the near-infrared region, the penetration may be increased to about 4-6 mm or more. To address the problem of penetration, interstitial PDT (IPDT) is being developed by many groups. Thin multiple optical fibres are inserted into a larger tumour mass and can thus be used for the treatment of thick tumours

(see Papers XIII, XIV) and tumours embedded in healthy tissue.

5.1.1 Photosensitizers

Sensitizers are fluorescent tumour-selective compounds that after excitation arrive in a triplet state, energetically positioned to allow energy transfer to molecular oxygen, which is promoted from the normal triplet ground state to the biologically very active singlet state, and becomes highly cytotoxic.

Hematoporphyrin derivative (HpD) was the substance that was almost exclusively used when PDT first was introduced. HpD is a mixture of different porphyrins and exhibits an absorption peak at 630 nm. However, HpD has some disadvantages such as long accumulation time, tumour selectivity of only 2-3 to 1, and the clearing time of HpD is quite long. Many second- and third-generation sensitizers are therefore being synthesised and are evaluated and/or used.

Right now, ALA-induced PpIX has attracted a lot of interest as photosensitizer. The idea of using ALA for PDT was introduced by Malik *et al.*¹⁰⁹ and Kennedy *et al.*^{110,111}. This new PDT modality was quickly adopted by the group in Lund⁷⁸. The accumulation of PpIX in tumour tissues was described in Chap. 4.2. The following discussion will be concentrated on the use of ALA-induced PpIX.

Recently, there has been a strong interest in esterified versions of ALA^{112,113}. By attaching a lipophilic carbon chain to the hydrophilic ALA, it may more easily penetrate the upper layers of the skin, which would give a deeper penetration depth of ALA in combination with reduced accumulation time. However, if the attached carbon chain is too long, ALA might get stuck in the upper layers and in addition esterases are required to detach the carbon chain before ALA can enter the haem cycle. Studies have been performed to determine the optimal length of chain and it has been shown that by attaching esters, the PpIX formation rate is higher for long-chained ALA esters than short-chained esters¹¹⁴. In Paper IX, it is shown that ALA-ME accumulates more selectively than ALA for basal cell carcinoma.

The stratum corneum acts like a barrier and the penetration of ALA through the stratum corneum can be enhanced by the use of iontophoresis¹¹⁵ or tape stripping. However, even if the penetration time is reduced, the formation of PpIX still requires several hours and since the stratum corneum of skin lesions is generally damaged, the clinical usefulness has to be evaluated.

5.1.2 Light

Any red light at 635 nm can be used for the treatment. High-power filtered lamps may be non-expensive, but the light economy is poor due to the rather narrow absorption peak of PpIX. In addition, these lamps produce a lot of heat and if the IR radiation is not filtered away, it can cause hyperthermic action, which may be a treatment modality in itself; however, unwanted in this situation.

The use of lasers is more convenient since the radiation can be matched to the absorption maximum of the photosensitizer and can easily be guided through optical

fibres to the treatment site. For superficial illumination, a microlens is attached to the distal end, creating a homogeneous light fluence at the surface, typically in the order of 100 mW/cm^2 . The light dose for treatment is calculated by multiplying the fluence rate with the illumination time used. For the treatment of basal cell carcinomas, a surface irradiation dose of 60 J/cm^2 is a commonly used light dose.

There is a potential risk of heating during PDT; however, the results of Paper X, show that the superficial tissue temperature is increased by only a few degrees for surface irradiation up to 150 mW/cm^2 .

5.1.3 Oxygen

Oxygen is transported by haemoglobin and is a prerequisite for PDT. However, oxygen is consumed during the process and it has been suggested that by fractionating the treatment illumination in time, the tissue can be re-oxygenated, which would lead to a more efficient use of the sensitizer and increase the tumour damage. Fractionation intervals between milliseconds and several hours have been suggested. In Paper XI, a few schemes of pulsed and continuous delivery modes were tested, but no significant difference could be found.

Some of the treatment mechanisms described below include vascular damage, which could limit further treatment due to restricted blood perfusion in the tumour. Also fast-growing tumours may be hypoxic. Oxygen is otherwise often assumed to be in excess. For the purpose of improving the understanding of the PDT mechanisms it would be interesting to monitor the oxygen content in the tumour during PDT.

5.1.4 Dosimetry

In order to optimise PDT for superficial and in particular interstitial application, the dosimetry should be fully understood and many reviews on the topic can be found in the literature¹¹⁶⁻¹¹⁹.

There are many steps involved in the process of creating the cytotoxic damage, which finally leads to tumour necrosis. In Fig. 19, the different steps involved are outlined. The light distribution can be predicted by the use of analytical or numerical methods, see Sect. 2.4, and for a more complete description, see Ref.⁶.

The distribution of ALA after topical administration, the conversion to PpIX and the subsequent distribution of PpIX can be modelled. There have been attempts by Svaasand *et al.*¹²⁰ to build a dosimetry model for ALA-PDT of topical lesions. The distribution of cytotoxic oxygen is predicted from the optical dose, the drug dose and the accumulation time. There is also another model by Star *et al.*¹²¹ to calculate the time-dependent PpIX concentration after topical application of ALA on skin. In this model, realistic boundary conditions are incorporated.

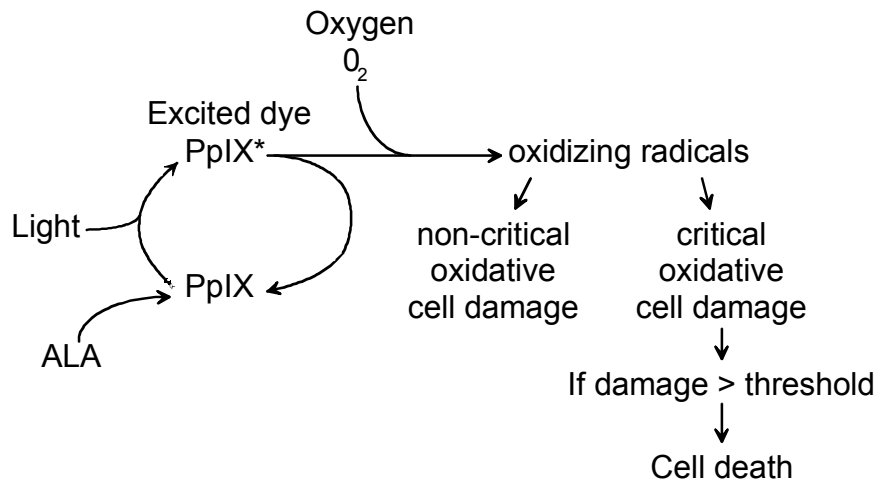


Figure 19. PDT dosimetry. Adapted from Jacques¹²².

The conversion of ALA to PpIX has been modelled by Aalders *et al.*¹²³ using a three-compartment model that takes into account the drug distribution, conversion to PpIX and the conversion to haem. The result shows that the PpIX kinetics in skin is strongly dependent on the concentration of ALA.

The distribution of PpIX after topical application of ALA can also be experimentally verified by fluorescence microscopy¹²⁴. In Fig 20, the fluorescence image of a basal cell carcinoma, measured with the confocal microscope at the Division of Atomic Physics, is shown.

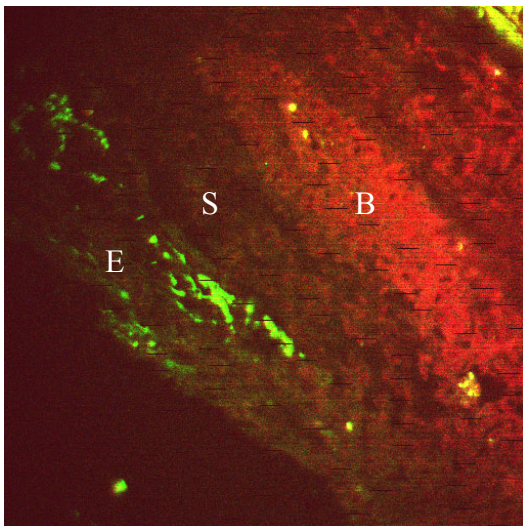


Figure 20. Fluorescence microscopy image of a basal cell carcinoma. The green autofluorescence of the epithelium (E) and stroma (S) can be seen together with the red PpIX fluorescence of the basal cell carcinoma (B) further down in the tissue.

The quantum yield of PpIX and the transfer rate to oxygen are important parameters and more information can be found in Refs.^{125,126}. Oxygen is consumed during the process and it has been shown that if the capillary density is not high enough, oxygen cannot be considered homogeneously distributed in excess¹²⁷. Depending on the cellular location of the photosensitizer, the damage of an oxidative reaction varies.

Normally, a very clear and distinct border between healthy tissue and necrotic tissue can be observed in micrographic slides after PDT. This has led to the conclusion that there must be some specific threshold, for which there has been a certain degree of damage from cytotoxic singlet oxygen radicals to a cell that causes it to die. However, this parameter is not easy to measure, instead, the parameter for photodynamic threshold dose is expressed as the number of photons absorbed by the photosensitizer per unit tissue volume that leads to cell necrosis. By this definition, only the distributions of light and photosensitizer are taken into account, the oxygen concentration is considered to be enough not to limit the process. The parameter has been estimated for various photosensitizers (mTHPC¹²⁸, Photofrin¹²⁹, ALPcS₁^{129,130}, and ALPcS₄¹²⁹), and in Paper XII, an estimation of the photodynamic threshold for PpIX is reported.

5.2 Treatment mechanisms

The creation of oxygen radicals and its subsequent damage to the cells is the primary treatment effect of PDT. However, there are also secondary effects, which significantly contribute to the treatment response.

5.2.1 Primary photodamage

Due to the short lifetime of the singlet oxygen, the localisation of the photosensitizer determines the type of damage to the cell. Lipophilic photosensitizers accumulate in the cell membranes and in the membranes of the cell organelles and photooxidation may lead to rupture and inactivation of enzymes and receptors. Hydrophilic photosensitizers are more likely to accumulate in lysosomes and endosomes^{131,132}. Photooxidation may lead to the release of lysosomal enzymes in the cytoplasm. Aggregated photosensitizers in the cytoplasm may bind to tubulin and the photooxygenation lead to de-polymerisation of microtubuli which subsequently lead to cell death, since the cells cannot go into mitosis¹³¹. It has been shown that the probability of cell death per quantum of absorbed energy is higher for lipophilic photosensitizers, indicating that membrane structures are more vulnerable¹³³.

5.2.2 Secondary effects

There are several secondary effects of the direct photodamage that contribute to the treatment efficacy. When systemic (oral or intravenous) administration of the sensitizer is used, a large amount will be localised in the endothelial cells of vessels and the treatment causes permanent damage^{134,135}. In Paper X, perfusion measurements were performed in connection with PDT of basal cell carcinomas and vascular effects were seen clearly.

The photooxidation will also lead to inflammatory and immunology responses^{136,137}

which may also contribute to the treatment efficacy. In addition, the induction of apoptosis, i.e. programmed cell death, may contribute to the treatment¹³⁸.

5.3 Clinical applications

PDT has a large number of different applications in several clinical specialities, mostly involving tumours of different origins, but also in the treatment of age-related macula degeneration and diabetic retinopathy. A review of clinical treatment results using ALA-PDT has been prepared by Peng *et al.*¹³⁹.

5.3.1 Topical PDT of skin lesions

Basal cell cancer (BCC) is the most common malignant skin lesion and it is the PDT response of this lesion type that is described in Papers IX-XI and XIV. Even if BCC is not considered highly malignant, it can still cause significant problems for the patient. The conventional treatment methods include excision, radiation, electrocoagulation and cryosurgery. The treatment choice depends on lesion location and type. In a randomised Phase III study, PDT was used versus cryotherapy and there were comparable treatment results but the cosmetic outcome of PDT was significantly better, and the healing time shorter¹⁴⁰.

The use of methyl-esterified ALA was evaluated in Paper IX. Due to its higher lipophilicity than ALA, it may penetrate the skin faster and a shorter accumulation time can be used.

Since oxygen is consumed during the PDT process, it has been suggested that the use of fractionated light would enhance the treatment effects since the tissue is allowed to re-oxygenate. This was evaluated using a laser emitting at 652 nm, see Paper XI, and the light dose was increased to compensate for the lower excitation efficiency at that wavelength. However, the study showed no significant differences between CW or modulated application.

5.3.2 Interstitial PDT

In order to be able to treat thick tumours and tumours embedded deeper in the body, an interstitial system has been constructed¹⁴¹. It has been used for experimental studies in a rat model (Paper XIII) and it has also been clinically evaluated *in vivo* on patients with thick nodular BCCs (Paper XIV).

The present system consists of a beam-splitting unit in which the incoming treatment light is divided into 6 output fibres. The optimal fibre positions are calculated by a finite element method that solves the diffusion equation for the given tumour geometry and tissue optical properties. In the first applications of the system, a delivered light dose of 15 J/cm³ was considered to be the threshold to induce tumour necrosis, which determines the illumination time. The system is capable of feed-back control during treatment since each fibre also can be used for the measurement of the light fluence inside the tumour. This is done by blocking the input to the treatment fibres with photodiodes. However, this possibility of treatment control has not been fully implemented yet.

Acknowledgements

First of all, I would like to thank my supervisor Stefan Andersson-Engels for inspiration, motivation and guidance through the project. I really appreciate all the fun we have had, especially during travels and measurement campaigns all over the world. I would also like to give Sune Svanberg my warmest thanks for rapid processing of manuscripts and also for his extremely enthusiastic inspiration, which is highly contagious. Katarina Svanberg has been my clinical mentor and I have learned a lot of interesting medicine from her, which I am very grateful for. In addition, I have really enjoyed her friendly company during travels and work during which there has always been time for spontaneous jokes and laugh-attacks. I would also thank the 'Danish skin doctor' Niels Bendsøe who has helped me a lot during clinical measurements. I have really enjoyed the precise pathology work together with Prof. em. Unne Stenram who has taught me a great deal about pink and purple cells and who has made valuable contributions to the scientific work.

My appreciation for the skilled technical personnel at the division, Åke Bergquist and Bertil Hermansson must be noted. Many thanks for their help with both analogue and digital electronics.

I have really enjoyed the interesting collaboration with the nice and friendly people at Science and Technology International, both during the Vilnius campaign, my visit and during the finalising of the manuscripts for this thesis. Mahalo nui loa!

I would also send my gratitude to former and present PhD students with whom it has been a pleasure to work with, or just to socialise with at work and to party with. My thanks go to Marcelo Soto Thompson, Thomas Johansson, Johannes Swartling, Petter Weibring, Eva Samsøe, Christoffer Abrahamsson, Ulf Gustafsson, Maria Stenberg, Ann Johansson, Claes af Klinteberg, Lotta Eker and Ingrid Wang.

Marcelo Soto Thompson, who has been my room-mate and always tries to cheer me up when things were bad, deserves a special friendly 'Thank You!' He never gets tired or irritated of my conservative way to reject all his wild suggestions at first.

My kindest appreciation and thanks to all of my friends who make my life interesting.

My family deserves a warm thank for all support of my work, even if they don't always understand it. My beloved Ulf has been very understanding and helpful and I give him all my love.

Summary of papers

Paper I reports on Raman spectroscopy measurements performed *in vivo* on various types of skin lesions. The results suggest that the resolution and intensity of the Raman peak do not allow a classification based on Raman spectra recorded in 5 seconds using 20 mW.

Paper II describes measurements of the optical properties of myocardium that had been subjected to radio-frequency ablation therapy. The results could aid in the development of an optical probe to guide such therapy in real-time.

Paper III presents fluorescence spectra recorded on biopsies from patients with transplanted hearts. Fibrous tissue could be distinguished compared to healthy myocardium. However, the number of biopsies was too low to allow characterization of rejected tissue.

Paper IV demonstrates a new fluorescence spectroscopy device based on a blue diode laser and a compact spectrometer.

Paper V describes fluorescence spectroscopy performed on brain tumours during stereotactical biopsy. The optical fibre was inserted through the biopsy needle and fluorescence spectra were recorded on both normal brain and tumour tissue.

Paper VI deals with a detailed histopathological protocol for cervical biopsies. The orientation, location and pathological variability within biopsies are recorded to allow correlation with optically recorded spectra.

Papers VII and VIII are connected with Paper VI as they all originate from the same clinical trial, where a fluorescence and reflectance imaging system was used for imaging of the cervix. In Paper VII, the correlation between fluorescence spectral shape and histopathological diagnosis is discussed. In Paper VIII, the spatial variation in the cervical images is calculated.

Paper IX contains a comparison of the diagnostic and therapeutic outcome when using topically applied methyl-esterified ALA and normal ALA in PDT of basal cell carcinoma lesions. Laser-induced fluorescence was used to monitor the build-up of PpIX and, in addition, the superficial perfusion and temperature was measured.

Paper X reports on measurements, that indirectly provide information on the vascular mechanisms during topical PDT. An infrared camera was used to measure the superficial temperature and the superficial perfusion was studied using a laser-Doppler instrument.

Paper XI describes the use of a diode laser emitting at 652 nm in PDT of skin lesions. The laser emission was tested in three different modes, continuous, pulsed and in a special mode developed by the laser manufacturer. No statistically valid differences were observed for the various treatment modes.

Paper XII reports on an estimation of the photodynamic threshold dose of PpIX.

Papers XIII and XIV report on the feasibility of an interstitial interactive system for PDT of malignant tumours. The system has been tested both in experimental studies on rats (Paper XIII) and in a clinical trial involving patients with thick skin lesions (Paper XIV).

Contribution by the author to the papers

- Paper I.** Major part of experimental work, data evaluation and manuscript preparation.
- Paper II.** Contribution to *in-vivo* measurements. Minor part of integrating sphere measurements and contribution to manuscript preparation.
- Paper III.** Major part of *in-vitro* measurements and data evaluation. Substantial part of manuscript preparation.
- Paper IV.** Substantial part of equipment assembling. Contributions to testing and manuscript preparation.
- Paper V.** Substantial part of *in-vivo* measurements. Major part of data evaluation and manuscript preparation.
- Paper VI.** Contribution to histopathological protocol design and evaluation. Major part of manuscript preparation.
- Paper VII.** Contribution to *in-vivo* measurements, data evaluation and manuscript preparation.
- Paper VIII.** Participation in the clinical trial. Evaluation of the histopathological information, which is used for the correlation between images and diagnostics.
- Paper IX.** Contribution to experimental work, data evaluation and manuscript preparation.
- Paper X.** Major part of measurements and data evaluation. Substantial part of manuscript preparation.
- Paper XI.** Contribution to measurements, data evaluation and manuscript preparation.
- Paper XII.** Substantial part of measurements. Major part of data evaluation and manuscript preparation.
- Paper XIII.** Contribution to measurements and manuscript preparation.
- Paper XIV.** Contribution to manuscript preparation.

References

1. H. Haken and H.C. Wolf, *The Physics of Atoms and Quanta*, (Springer-Verlag, Berlin, Germany, 1994).
2. H. Friedrich, *Theoretical Atomic Physics*, (Springer Verlag, Heidelberg, Germany, 1998).
3. S. Svanberg, *Atomic and Molecular Spectroscopy – Basic Aspects and Practical Applications*, (Springer Verlag, Heidelberg, Germany, 2001).
4. C. Eker, Optical characterization of tissue for medical diagnostics, Dissertation thesis, Lund Institute of Technology, Lund, Sweden (1999).
5. J.-L. Boulnois, Photophysical processes in recent medical laser developments: a review, *Lasers Med. Sci.* **1**, 47-66 (1986).
6. A.J. Welch and M.J.C. van Gemert, *Optical-Thermal Response of Laser-Irradiated Tissue*, (Plenum Press, New York, NY, 1995).
7. C. Sturesson, Medical laser-induced thermotherapy - models and applications, Dissertation thesis, Lund Institute of Technology, Lund, Sweden (1998).
8. L.E. Gerweck, Hyperthermia in cancer therapy: the biological basis and unresolved questions, *Cancer Res.* **45**, 3408-3414 (1985).
9. W.C. Dewey, Arrhenius relationships from the molecule and cell to the clinic, *Int. J. Hyperthermia* **10**, 457-483 (1994).
10. J. Beuthan, O. Minet, J. Helfmann, M. Herrig and G. Müller, The spatial variation of the refractive index in biological cells, *Phys. Med. Biol.* **41**, 369-382 (1996).
11. J.R. Mourant, T.M. Johnson, V. Doddi and J.P. Freyer, Angular dependent light scattering from multicellular spheroids, *J. Biomedical Optics* **7**, 93-99 (2002).
12. B. Beauvoit, S.M. Evans, T.W. Jenkins, E.E. Miller and B. Chance, Correlation between the light scattering and the mitochondrial content of normal tissues and transplantable rodent tumors, *Anal. Biochem.* **226**, 167-174 (1995).
13. R.A.J. Groenhuis, H.A. Ferwerda and J.J. ten Bosch, Scattering and absorption of turbid materials determined from reflection measurements. 1: Theory, *Appl. Opt.* **22**, 2456-2462 (1983).
14. J.R. Mourant, T. Fuselier, J. Boyer, T.M. Johnson and I.J. Bigio, Predictions and measurements of scattering and absorption over broad wavelength ranges in tissue phantoms, *Appl. Opt.* **36**, 949-957 (1997).
15. I.J. Bigio, S.G. Bown, C. Kelley, S. Lakhani, D. Pickard, P.M. Ripley, I.G. Rose and C. Saunders, Diagnosis of breast cancer using elastic-scattering spectroscopy: preliminary clinical results, *J. Biomedical Optics* **5**, 221-228 (2000).
16. M.S. Patterson, B. Chance and B.C. Wilson, Time resolved reflectance and transmittance for the non-invasive measurement of optical properties, *Appl. Opt.* **28**, 2331-2336 (1989).

17. M.S. Patterson, J.D. Moulton, B.C. Wilson, K.W. Berndt and J.R. Lakowicz, Frequency-domain reflectance for the determination of the scattering and absorption properties of tissue, *Appl. Opt.* **30**, 4474-4476 (1991).
18. N. Shah, A. Cerussi, C. Eker, J. Espinoza, J. Butler, J. Fishkin, R. Hornung and B. Tromberg, Noninvasive functional optical spectroscopy of human breast tissue, *Proc. Natl. Acad. Sci. USA* **98**, 4420-4425 (2001).
19. R. Cubeddu, A. Pifferi, P. Taroni, A. Torricelli and G. Valentini, Noninvasive absorption and scattering spectroscopy of bulk diffusive media: An application to the optical characterization of human breast, *Appl. Phys. Lett.* **74**, 874-876 (1999).
20. K. Wårdell and G. Nilsson, Laser Doppler imaging of skin, in *Non-invasive methods and the skin*, eds. J. Serup and B.E. Jemec, pp. 421-427 (CRC Press, Boca Raton, 1995).
21. W.M. Star, Diffusion theory of light transport, in *Optical-Thermal Response of Laser-Irradiated Tissue*, eds. A.J. Welch and M.J.C. van Gemert, pp. 131-206 (Plenum Press, New York, 1995).
22. L. Wang and S.L. Jacques, Monte Carlo modeling of light transport in multi-layered tissues in standard C, (Laser Biology Research Laboratory, M. D. Anderson Cancer Center, University of Texas, Houston, Texas 1992).
23. L. Wang, S.L. Jacques and L. Zheng, MCML - Monte Carlo modeling of light transport in multi-layered tissues, *Computer Methods and Programs in Biomedicine* **47**, 131-146 (1995).
24. S.A. Prahl, The adding-doubling method, in *Optical-Thermal Response of Laser-Irradiated Tissue*, eds. A.J. Welch and M.J.C. van Gemert, pp. 101-129 (Plenum Press, New York, 1995).
25. R.H. Clarke, J.M. Isner, T. Gauthier, K. Nakagawa, F. Cerio, E. Hanlon, E. Gaffney, E. Rouse and S. DeJesus, Spectroscopic characterization of cardiovascular tissue, *Lasers Surg. Med.* **8**, 45-59 (1988).
26. R.R. Alfano, A. Pradhan, G.C. Tang and S.J. Wahl, Optical spectroscopic diagnosis of cancer and normal breast tissues, *J. Opt. Soc. Am. B* **6**, 1015-1023 (1989).
27. R. Manoharan, Y. Wang and M.S. Feld, Histochemical analysis of biological tissues using Raman spectroscopy, *Spectrochim. Acta* **52**, 215-249 (1995).
28. E.B. Hanlon, R. Manoharan, T.W. Koo, K.E. Shafer, J.T. Motz, M. Fitzmaurice, J.R. Kramer, I. Itzkan, R.R. Dasari and M.S. Feld, Prospects for in vivo Raman spectroscopy, *Phys. Med. Biol.* **45**, 1-59 (2000).
29. A. Mahadevan-Jensen and R. Richards-Kortum, Raman spectroscopy for the detection of cancers and precancers, *J. Biomedical Optics* **1**, 31-70 (1996).
30. L.-P. Choo-Smith, H.G.M. Edwards, H.P. Endtz, J.M. Kros, F. Heule, H. Barr, J.S. Robinson, H.A. Bruining and G.J. Puppels, Medical applications of Raman spectroscopy: From proof of principle to clinical implementation, *Biospectroscopy* **67**, 1-9 (2002).

31. J.F. Brennan, T.J. Römer, R.S. Lees, A.M. Tercyak, J.R. Kramer and M.S. Feld, Determination of human coronary artery composition by Raman spectroscopy, *Circulation* **96**, 99-105 (1997).
32. T.J. Römer, J.F. Brennan, M. Fitzmaurice, M.L. Feldstein, G. Deinum, J.L. Myles, J.R. Kramer, R.S. Lees and M.S. Feld, Histopathology of human coronary atherosclerosis by quantifying its chemical composition with Raman spectroscopy, *Circulation* **97**, 878-885 (1998).
33. T.J. Römer, J.F. Brennan, T.C. Bakker Schut, R. Wolthuis, R.C.M. van den Hoogen, J.J. Emeis, A. van der Laarse, A.V.G. Brusckhe and G.J. Puppels, Raman spectroscopy for quantifying cholesterol in intact coronary artery wall, *Atherosclerosis* **141**, 117-124 (1998).
34. H.P. Buschman, E.T. Marple, M.L. Wach, B. Bennett, T.C. Bakker Schut, H.A. Bruining, A.V. Brusckhe, A. van der Laarse and G.J. Puppels, In vivo determination of the molecular composition of artery wall by intravascular Raman spectroscopy, *Anal. Chem.* **72**, 3771-3775 (2000).
35. P.J. Caspers, G.W. Lucassen, E.A. Carter, H.A. Bruining and G.J. Puppels, In vivo confocal Raman microspectroscopy of the skin: noninvasive determination of molecular concentration profiles, *J. Invest. Dermatol.* **116**, 434-442 (2001).
36. J.Y. Qu, B.C. Wilson and D. Suria, Concentration measurements of multiple analytes in human sera by near-infrared laser Raman spectroscopy, *Appl. Opt.* **38**, 5491-5498 (1999).
37. A.J. Berger, T.W. Koo, I. Itzkan, G. Horowitz and M.S. Feld, Multicomponent blood analysis by near-infrared Raman spectroscopy, *Appl. Opt.* **38**, 2916-2926 (1999).
38. P. Weinmann, M. Jouan, Nguyen Quy Dao, B. Lacroix, C. Groiselle, J.-P. Bonte and G. Luc, Quantitative analysis of cholesterol and cholesteryl esters in human atherosclerotic plaques using near-infrared Raman spectroscopy, *Atherosclerosis* **140**, 81-88 (1998).
39. M. Gniadecka, H.C. Wulf, O.F. Nielsen, D.H. Christensen and J. Hercogova, Distinctive molecular abnormalities in benign and malignant skin lesions: studies by Raman spectroscopy, *Photochem. Photobiol.* **66**, 418-423 (1997).
40. S. Fendel and B. Schrader, Investigation of skin and skin lesions by NIR-FT Raman spectroscopy, *Fresenius J. Anal. Chem.* **360**, 609-613 (1998).
41. M. Gniadecka, H.C. Wulf, N. Nymark-Mortensen, O. Faurskov-Nielsen and D.H. Christensen, Diagnosis of basal cell carcinoma by Raman spectroscopy, *Journal of Raman Spectroscopy* **28**, 125-129 (1997).
42. A. Nijssen, T.C. Bakker Schut, F. Heule, P.J. Caspers, D.P. Hayes, M.H.A. Neumann and G.J. Puppels, Discriminating basal cell carcinoma from its surrounding tissue by Raman spectroscopy, *J. Invest. Dermatol.* **119**, 64-69 (2002).

43. R. Manoharan, K. Shafer, L. Perelman, J. Wu, K. Chen, G. Deinum, M. Fitzmaurice, J. Myles, J. Crowe, R.R. Dasari and M.S. Feld, Raman spectroscopy and fluorescence photon migration for breast cancer diagnosis and imaging, *Photobiochem. Photobiophys.* **67**, 15-22 (1998).
44. A. Mahadevan-Jensen, M.F. Mitchell, N. Ramanujam, A. Malpica, S. Thomsen, U. Utzinger and R. Richards-Kortum, Near-Infrared Raman spectroscopy for in vitro detection of cervical precancers, *Photochem. Photobiol.* **68**, 123-132 (1998).
45. M.G. Shim, L.M. Song, N.E. Marcon and B.C. Wilson, In vivo near-infrared Raman spectroscopy: demonstration of feasibility during clinical gastrointestinal endoscopy, *Photochem. Photobiol.* **72**, 146-150 (2000).
46. M.G. Shim and B.C. Wilson, The effects of ex vivo handling procedures on the near-infrared Raman spectra of normal mammalian tissues, *Photochem. Photobiol.* **63**, 662-671 (1996).
47. J.J. Baraga, M.S. Feld and R.P. Rava, In situ optical histochemistry of human artery using near infrared Fourier transform Raman spectroscopy, *Proc. Natl. Acad. Sci. USA* **89**, 3473-3477 (1992).
48. R. Manoharan, J.J. Baraga, R.P. Rava, R.R. Dasari, M. Fitzmaurice and M.S. Feld, Biochemical analysis and mapping of atherosclerotic human artery using FT-IR microspectroscopy, *Atherosclerosis* **103**, 181-193 (1993).
49. S. Keller, B. Schrader, A. Hoffman, W. Schrader, K. Metz, A. Rehlaender, J. Pahnke, M. Ruwe and W. Budach, Application of near-infrared-Fourier transform Raman spectroscopy in medical research, *Journal of Raman Spectroscopy* **25**, 663-671 (1994).
50. J.J. Baraga, M.S. Feld and R.P. Rava, Rapid near-infrared Raman spectroscopy of human tissue with a spectrograph and CCD detector, *Appl. Spectr.* **46**, 187-190 (1992).
51. M.G. Shim and B.C. Wilson, Development of an in vivo Raman spectroscopic system for diagnostic applications, *Journal of Raman Spectroscopy* **28**, 131-142 (1997).
52. P.J. Caspers, G.W. Lucassen, R. Wolthuis, H.A. Bruining and G.J. Puppels, In vitro and in vivo Raman spectroscopy of human skin, *Biospectroscopy* **4**, 31-39 (1998).
53. J.R. Kramer, J.F. Brennan, T.J. Römer, Y. Wang, R.R. Dasari and M.S. Feld, Spectral diagnosis of human coronary artery: A clinical system for real time analysis, in *Lasers in Surgery: Advanced Characterization, Therapeutics, and Systems V*, ed. R.R. Anderson, Proc. SPIE vol. **2395**, 376-382 (1995).
54. J.F. Brennan, Y. Wang, R.R. Dasari and M.S. Feld, Near-infrared Raman spectrometer systems for human tissue studies, *Appl. Spectr.* **51**, 201-208 (1997).
55. A. Mahadevan-Jensen, M.F. Mitchell, N. Ramanujam, U. Utzinger and R. Richards-Kortum, Development of a fiber optic probe to measure NIR Raman spectra of cervical tissue in vivo, *Photochem. Photobiol.* **68**, 427-431 (1998).

56. C.J. Frank, D.C.B. Redd, T.S. Gansler and R.L. McCreery, Characterization of human breast biopsy specimens with near-IR Raman spectroscopy, *Anal. Chem.* **66**, 319-326 (1994).
57. R. Manoharan, Y. Wang, R.R. Dasari, S.S. Singer, R.P. Rava and M.S. Feld, Ultraviolet resonance Raman spectroscopy for detection of colon cancer, *Lasers Life Sci.* **6**, 217-226 (1995).
58. J. Swartling, J.S. Dam and S. Andersson-Engels, Comparison of spatially and temporally resolved diffuse-reflectance measurement systems for determination of biomedical optical properties, submitted to *Applied Optics* (2002).
59. B. Araya and H. Malm, Raman spectroscopy for tissue characterization, Master's thesis, Lund Institute of Technology, Lund, Sweden (2000).
60. M.G. Shim, B.C. Wilson, E. Marple and M. Wach, Study of fiber-optic probes for in vivo medical Raman spectroscopy, *Appl. Spectr.* **53**, 619-627 (1999).
61. P.A. Mosier-Boss, S.H. Liebermann and R. Newbery, Fluorescence rejection in Raman spectroscopy by shifted-spectra, edge detection and FFT filtering techniques, *Appl. Spectr.* **49**, 630-638 (1995).
62. A. Malmberg, Fluorescence rejection in Raman spectroscopy by local polynomial kernel regression, Master Thesis, Department of Mathematical Statistics, Lund Institute of Technology, Lund, Sweden (1998).
63. A.J. Berger, T.W. Koo, I. Itzkan and M.S. Feld, An enhanced algorithm for linear multivariate calibration, *Anal. Chem.* **70**, 623-627 (1998).
64. A. Mizuno, H. Kitajima, K. Kawauchi, S. Muraishi and Y. Ozaki, Near-infrared Fourier transform Raman spectroscopic study of human brain tissues and tumours, *Journal of Raman Spectroscopy* **25**, 25-29 (1994).
65. T.J. Römer, J.F. Brennan, G.J. Puppels, A.H. Zwinderman, S.G. van Duinen, A. van der Laarse, A.F.W. van der Steen, N.A. Bom and A.V.G. Brusckhe, Intravascular ultrasound combined with Raman spectroscopy to localise and qualify cholesterol and calcium salts in atherosclerotic coronary arteries, *Atheroscler. Thromb. Vasc. Biol.* **20**, 478-483 (2000).
66. J.P. Salenius, J.F. Brennan, A. Miller, Y. Wang, T. Aretz, B. Sacks, R.R. Dasari and M.S. Feld, Biochemical composition of human peripheral arteries examined with near-infrared Raman spectroscopy, *J. Vasc. Surg.* **27**, 710-719 (1998).
67. S. Pålsson, M. Pålsson, S. Montán, K. Svanberg, S. Andersson-Engels, A. Malmberg, U. Holst, G. Zacharakis, G. Filippidis, T.G. Papazoglou, A. Katsamouris, R. Doornbos, R. van Veen, H.J.C.M. Sterenborg, G. Koduri and F. Cross, NIR Raman spectroscopy for cardiovascular tissue characterisation, *CLEO/Europe - EQEC Focus Meetings*, München, Germany, (1999).
68. B.W. Barry, H.G.M. Edwards and A.C. Williams, Fourier transform Raman and infrared vibrational study of human skin: assignment of spectral bands, *Journal of Raman Spectroscopy* **23**, 641-645 (1992).

69. M. Gniadecka, O.F. Nielsen, S. Wessel, M. Heidenheim, D.H. Christensen and H.C. Wulf, Water and protein structure in photoaged and chronically aged skin, *J. Invest. Dermatol.* **11**, 1129-1133 (1998).
70. M. Gniadecka, O.F. Nielsen, D.H. Christensen and H.C. Wulf, Structure of water, proteins and lipids in intact human skin, hair and nail, *J. Invest. Dermatol.* **110**, 393-399 (1998).
71. M. Gniadecka, H.C. Wulf, O. Faurskov-Nielsen, D.H. Christensen and J.P. Hart-Hansen, Fourier transform Raman spectroscopy of 15th century mummies from Qilakitsoq, Greenland, *Journal of Raman Spectroscopy* **28**, 179-184 (1997).
72. A.E. Profio, D.R. Doiron and J. Sarnaik, Fluorometer for endoscopic diagnosis of tumors, *Med. Phys.* **11**, 516-520 (1984).
73. S. Andersson-Engels, A. Gustafson, J. Johansson, U. Stenram, K. Svanberg and S. Svanberg, Investigation of possible fluorophores in human atherosclerotic plaque, *Lasers Life Sci.* **5**, 1-11 (1992).
74. J. Johansson, Fluorescence spectroscopy for medical and environmental diagnostics, Dissertation thesis, Lund Institute of Technology, Lund, Sweden (1993).
75. S. Andersson-Engels and B.C. Wilson, *In vivo* fluorescence in clinical oncology: Fundamental and practical issues, *J. Cell Pharmacol.* **3**, 48-61 (1992).
76. J. Ankerst, S. Montán, K. Svanberg and S. Svanberg, Laser-induced fluorescence studies of hematoporphyrin derivative (HpD) in normal and tumor tissue of rat, *Appl. Spectr.* **38**, 890-896 (1984).
77. S. Andersson-Engels, L. Baert, R. Berg, M.A. D'Hallewin, J. Johansson, U. Stenram, K. Svanberg and S. Svanberg, Fluorescence characteristics of human atherosclerotic plaque and malignant tumors, in *Optical Methods for Tumor Treatment and Early Diagnosis: Mechanisms and Techniques*, ed. T.J. Dougherty, Proc. SPIE vol. **1426**, 31-43 (1991).
78. K. Svanberg, T. Andersson, D. Killander, I. Wang, U. Stenram, S. Andersson-Engels, R. Berg, J. Johansson and S. Svanberg, Photodynamic therapy of non-melanoma malignant tumours of the skin using topical δ -amino levulinic acid sensitization and laser irradiation, *Br. J. Dermatol.* **130**, 743-751 (1994).
79. R.J. Nordstrom, L. Burke, J.M. Niloff and J.F. Myrtle, Identification of cervical intraepithelial neoplasia (CIN) using UV-excited fluorescence and diffuse-reflectance tissue spectroscopy, *Lasers Surg. Med.* **29**, 118-127 (2001).
80. R. Rydell, C. Eker, S. Andersson-Engels, P. Wahlberg and K. Svanberg, Fluorescence investigations to identify laryngeal lesions in vivo, Manuscript in preparation for Head and Neck (2002).
81. D.L. Heintzelman, R. Lotan and R. Richards-Kortum, Characterisation of the autofluorescence of polymorphonuclear leukocytes, mononuclear leukocytes and cervical epithelial cancer cells for improved spectroscopic discrimination of inflammation from dysplasia, *Photochem. Photobiol.* **71**, 327-332 (2000).

82. B. Chance and B. Schoener, Fluorometric studies of flavin component of respiratory chain, in *Flavins and flavoproteins*, ed. Slater, pp. 510-519 (Elsevier Publishing Comp, New York, USA, 1966).
83. R.C. Benson, R.A. Meyer, M.E. Zaruba and G.M. McKhann, Cellular autofluorescence - is it due to flavins?, *J. Histochem. Cytochem.* **27**, 44-48 (1979).
84. M. Tsuchida, T. Miura and K. Aibara, Lipofuscin and lipofuscin-like substances, *Chemistry and Physics of Lipids* **44**, 297-325 (1987).
85. R.R. Alfano, D.B. Tata, J. Cordero, P. Tomashefsky, F.W. Longo and M.A. Alfano, Laser induced fluorescence spectroscopy from native cancerous and normal tissue, *IEEE J. Quant. Electr.* **QE-20**, 1507-1511 (1984).
86. Y. Yang, Y. Ye, F. Li, Y. Li and P. Ma, Characteristic autofluorescence for cancer diagnosis and its origin, *Lasers Surg. Med.* **7**, 528-532 (1987).
87. S. Andersson-Engels, J. Johansson, U. Stenram, K. Svanberg and S. Svanberg, Malignant tumor and atherosclerotic plaque diagnosis using laser-induced fluorescence, *IEEE J. Quant. Electr.* **26**, 2207-2217 (1990).
88. A. Bogaards, M.C. Aalders, A.J.L. Jongen, E. Dekker and H.J.C.M. Sterenberg, Double ratio fluorescence imaging for the detection of early superficial cancers, *Rev. Sci. Instrum.* **72**, 3956-3961 (2001).
89. M.G. Muller, I. Georgakoudi, Q. Zhang, J. Wu and M.S. Feld, Intrinsic fluorescence spectroscopy in turbid media: disentangling effects of scattering and absorption, *Appl. Opt.* **40**, 4633-4646 (2001).
90. C. af Klinteberg, On the use of light for the characterization and treatment of malignant tumours, Dissertation thesis, Lund Institute of Technology, Lund, Sweden (1999).
91. I. Wang, Photodynamic therapy and laser-based diagnostic studies of malignant tumours, Dissertation thesis, Lund University, Lund, Sweden (1999).
92. M. Kondo, N. Hirota, T. Takaoka and M. Kajiwara, Heme-biosynthetic enzyme activities and porphyrin accumulation in normal liver and hepatoma cell lines of rat, *Cell Biol. Toxicol.* **9**, 95-105 (1993).
93. P. Hinnen, F.W.M. de Rooij, M.L.F. van Velthuysen, A. Edixhoven, R. van Hillegersberg, H.W. Tilanus, J.H.P. Wilson and P.D. Siersema, Biochemical basis of 5-aminolaevulinic acid-induced protoporphyrin IX accumulation: a study in patients with (pre)malignant lesions of the oesophagus, *Br. J. Cancer* **78**, 679-682 (1998).
94. C. af Klinteberg, A.M.K. Enejder, I. Wang, S. Andersson-Engels, S. Svanberg and K. Svanberg, Kinetic fluorescence studies of 5-aminolaevulinic acid-induced protoporphyrin IX accumulation in basal cell carcinomas, *J. Photochem. Photobiol. B* **49**, 120-128 (1999).
95. J.J. Baraga, P. Taroni, Y.D. Park, K. An, A. Maestri, L.L. Tong, R.P. Rava, C. Kittrell, R.R. Dasari and M.S. Feld, Ultraviolet laser induced fluorescence of human aorta, *Spectrochim. Acta* **45A**, 95-99 (1989).

96. L.I. Deckelbaum, M.L. Stetz, K.M. O'Brien, F.W. Cutruzzola, A.F. Gmitro, L.I. Laifer and G.R. Gindi, Fluorescence spectroscopy guidance of laser ablation of atherosclerotic plaque, *Lasers Surg. Med.* **9**, 205-214 (1989).
97. K.T. Schomacker, J.K. Frisoli, C.C. Compton, T.J. Flotte, J.M. Richter, T.F. Deutsch and N.S. Nishioka, Ultraviolet laser-induced fluorescence of colonic polyps, *Gastroenterology* **102**, 1155-1160 (1992).
98. S. Andersson-Engels, Å. Elner, J. Johansson, S.-E. Karlsson, L.G. Salford, L.-G. Strömblad, K. Svanberg and S. Svanberg, Clinical recording of laser-induced autofluorescence spectra for evaluation of tumour demarcation feasibility in selected clinical specialities, *Lasers in Med. Sci.*, (1988).
99. C. af Klinteberg, M. Andreasson, O. Sandström, S. Andersson-Engels and S. Svanberg, Compact medical fluorosensor for minimally invasive tissue characterisation, Submitted to *Rev. Sci. Instrum.* (2002).
100. S. Montán, K. Svanberg and S. Svanberg, Multi-color imaging and contrast enhancement in cancer tumor localization using laser-induced fluorescence in hematoporphyrin derivative (HpD)-bearing tissue, *Opt. Lett.* **10**, 56-58 (1985).
101. K. Svanberg, I. Wang, S. Colleen, I. Idvall, C. Ingvar, R. Rydell, D. Jocham, H. Diddens, S. Bown, G. Gregory, S. Montán, S. Andersson-Engels and S. Svanberg, Clinical multi-colour fluorescence imaging of malignant tumours - initial experience, *Acta Radiol.* **39**, 2-9 (1998).
102. Z. Malik, M. Dishi and Y. Garini, Fourier transform multipixel spectroscopy and spectral imaging of protoporphyrin in single melanoma cells, *Photochem. Photobiol.* **63**, 608-614 (1996).
103. R. Cubeddu, F. Docchio, W.Q. Liu, R. Ramponi and P. Taroni, A system for time-resolved laser fluorescence spectroscopy with multiple picosecond gating, *Rev. Sci. Instrum.* **59**, 2254-2259 (1988).
104. O.J. Balchum, A.E. Profio, D.R. Doiron and G.C. Huth, Imaging fluorescence bronchoscopy for localizing early bronchial cancer and carcinoma in situ, *Prog. Clin. Biol. Res.* **170**, 847-861 (1984).
105. R. Baumgartner, H. Fisslinger, D. Jocham, H. Lenz, L. Ruprecht, H. Stepp and E. Unsold, A fluorescence imaging device for endoscopic detection of early stage cancer--instrumental and experimental studies, *Photochem. Photobiol.* **46**, 759-763 (1987).
106. G. Wagnières, C. Depeursinge, P. Monnier, M. Savary, P. Cornaz, A. Châtelain and H. van den Bergh, Photodetection of early cancer by laser induced fluorescence of a tumour-selective dye: apparatus design and realization, in *Photodynamic Therapy: Mechanisms II*, Proc. SPIE **1203**, 43-52 (1990).
107. S. Andersson-Engels, K. Svanberg and S. Svanberg, Fluorescence imaging in medical diagnostics, in *Biomedical Optics*, ed. J. Fujimoto, (2003).
108. J. Ekström, Development of software for a diode-based fluorosensor, Master thesis, Department of Physics, Lund Institute of Technology, Lund, Sweden (2002).

109. Z. Malik and H. Lugaci, Destruction of erythroleukaemic cells by photoinactivation of endogenous porphyrins, *Br. J. Cancer* **56**, 589-595 (1987).
110. J.C. Kennedy, R.H. Pottier and D.C. Pross, Photodynamic therapy with endogenous protoporphyrin IX: Basic principles and present clinical experience, *J. Photochem. Photobiol. B* **6**, 143-148 (1990).
111. J.C. Kennedy and R.H. Pottier, Endogenous protoporphyrin IX, a clinically useful photosensitizer for photodynamic therapy, *J. Photochem. Photobiol. B* **14**, 275-292 (1992).
112. J. Moan, L.W. Ma and V. Iani, On the pharmacokinetics of topically applied 5-aminolevulinic acid and two of its esters, *Int. J. Cancer* **92**, 139-143 (2001).
113. J.T.H.M. van den Akker, V. Iani, W.M. Star, H.J.C.M. Sterenborg and J. Moan, Topical application of 5-aminolevulinic acid hexyl ester and 5-aminolevulinic acid to normal nude mouse skin: Differences in protoporphyrin IX fluorescence kinetics and the role of the stratum corneum, *Photochem. Photobiol.* **72**, 681-689 (2000).
114. P. Uehlinger, M. Zellweger, G. Wagnieres, L. Juillerat-Jeanneret, H. van den Bergh and N. Lange, 5-Aminolevulinic acid and its derivatives: physical chemical properties and protoporphyrin IX formation in cultured cells, *J. Photochem. Photobiol. B* **54**, 72-80 (2000).
115. H.E. Boddé, P.E.H. Roemelé and W.M. Star, Quantification of topically delivered 5-aminolevulinic acid by iontophoresis across *ex vivo* human stratum corneum, *Photochem. Photobiol.* **75**, 418-423 (2002).
116. W.M. Star, B.C. Wilson and M.S. Patterson, Light delivery and optical dosimetry in photodynamic therapy of solid tumors, in *Photodynamic Therapy*, ed. B.W. Henderson, pp. 335-367, (New York; Basel; Hong Kong, 1992).
117. L.I. Grossweiner, PDT light dosimetry revisited, *J. Photochem. Photobiol. B* **38**, 258-268 (1997).
118. B.C. Wilson, M.S. Patterson and L. Lilje, Implicit and explicit dosimetry in photodynamic therapy: a new paradigm, *Lasers Med. Sci.* **12**, 182-199 (1997).
119. W.M. Star, Light dosimetry *in vivo*, *Phys. Med. Biol.* **42**, 763-787 (1997).
120. L.O. Svaasand, P. Wyss, M.T. Wyss, Y. Tadir, B.J. Tromberg and M.W. Berns, Dosimetry model for photodynamic therapy with topically administered photosensitizers, *Lasers Surg. Med.* **18**, 139-149 (1996).
121. W.M. Star, M.C.G. Aalders, A. Sac and H.J.C.M. Sterenborg, Quantitative model calculation of the time-dependent protoporphyrin IX concentration in normal human epidermis after delivery of ALA by passive topical application and iontophoresis, *Photochem. Photobiol.* **75**, 424-432 (2002).
122. S.L. Jacques. The mathematics of PDT dosimetry for cancer treatment. <http://www.omlc.ogi.edu/pdt/articles/PDTmath/index.html> (1998).
123. M.C.G. Aalders, N. van der Vange, W.M. Star and H.J.C.M. Sterenborg, A mathematical evaluation of dose-dependent PpIX fluorescence kinetics *in vivo*, *Photochem. Photobiol.* **74**, 311-317 (2001).

124. Q. Peng, T. Warloe, J. Moan, H. Heyerdahl, H.B. Steen, J.M. Nesland and K.-E. Giercksky, Distribution of 5-aminolevulinic acid-induced porphyrins in noduloulcerative basal cell carcinoma, *Photochem. Photobiol.* **62**, 906-913 (1995).
125. B.J. Tromberg, A. Orenstein, S. Kimel, S.J. Barker, J. Hyatt, J.S. Nelson and M.W. Berns, In vivo tumor oxygen tension measurements for the evaluation of the efficiency of photodynamic therapy, *Photochem. Photobiol.* **52**, 375-385 (1990).
126. T.H. Foster, R.S. Murant, R.G. Bryant, R.S. Knox, S.L. Gibson and R. Hilf, Oxygen consumption and diffusion effects in photodynamic therapy, *Radiat. Res.* **126**, 296-303 (1991).
127. T.H. Foster and L. Gao, Dosimetry in photodynamic therapy: oxygen and the critical importance of capillary density, *Radiat. Res.* **130**, 379-383 (1992).
128. S. Andrejevic-Blant, A. Woodtli, G. Wagnieres, C. Fontolliet, H. van den Bergh and P. Monnier, Interstitial photodynamic therapy with tetra(m-hydroxyphenyl)chlorin: tumor versus striated muscle damage, *Int. J. Radiat. Oncol. Biol. Phys.* **42**, 403-412 (1998).
129. T.J. Farrell, B.C. Wilson, M.S. Patterson and M.C. Olivo, Comparison of the in vivo photodynamic threshold dose of Photofrin, mono- and tetrasulfonated aluminum phthalocyanine using a rat liver model, *Photochem. Photobiol.* **68**, 394-399 (1998).
130. M.S. Patterson, B.C. Wilson and R. Graff, In vivo tests of the concept of photodynamic threshold dose in normal rat liver photosensitized by aluminum chlorosulphonated phthalocyanine, *Photochem. Photobiol.* **51**, 343-349 (1990).
131. K. Berg and J. Moan, Lysosomes and microtubules as targets for photochemotherapy of cancer, *Photochem. Photobiol.* **65**, 403-409 (1997).
132. K.W. Woodburn, Q. Fan, D.R. Miles, D. Kessel, Y. Luo and S.W. Young, Localisation and efficacy analysis of the phototherapeutic lutetium texaphyrin (PCI-0123) in the murine EMT6 sarcoma model, *Photochem. Photobiol.* **65**, 410-415 (1997).
133. T.J. Dougherty and S.L. Marcus, Photodynamic therapy, *Eur. J. Cancer* **28A**, 1734-1742 (1992).
134. V.H. Fingar, T.J. Wieman, S.A. Wiehle and P.B. Cerrito, The role of microvascular damage in photodynamic therapy: The effect of treatment on vessel constriction, permeability and leukocyte adhesion, *Cancer Res.* **52**, 4914-4921 (1992).
135. D.L. Liu, I. Wang, S. Andersson-Engels, C.H. Håkansson, U. Stenram and K. Svanberg, Intra-operative laser-induced photodynamic therapy in the treatment of experimental hepatic tumours, *Eur. J. Gastroenterol. Hepatol.* **7**, 1073-1080 (1995).
136. M. Korbelik, Induction of tumor immunity by photodynamic therapy, *J. Clin. Laser Med. Surg.* **14**, 329-334 (1996).

137. G. Krosł, M. Korbelik, J. Krosł and G.J. Dougherty, Potentiation of photodynamic therapy-elicited antitumour response by localized treatment with granulocyte-macrophage colony-stimulating factor, *Cancer Res.* **56**, 3281-3286 (1996).
138. M.L. Agarwal, M.E. Clay, E.J. Harvey, H.H. Evans, A.R. Antunez and N.L. Oleinick, Photodynamic therapy induces rapid cell death by apoptosis in L5178Y mouse lymphoma cells, *Cancer Res.* **51**, 5993-5996 (1991).
139. Q. Peng, T. Warloe, K. Berg, J. Moan, M. Kongshaug, K.-E. Giercksky and J.M. Nesland, 5-aminolevulinic acid-based photodynamic therapy: Clinical research and future challenges, *Cancer* **79**, 2282-2308 (1997).
140. I. Wang, N. Bendsoe, C. af Klinteberg, A.M.K. Enejder, S. Andersson-Engels, S. Svanberg and K. Svanberg, Photodynamic therapy versus cryosurgery of basal cell carcinomas; results of a phase III randomized clinical trial, *Br. J. Dermatol.* **144**, 832-840 (2001).
141. T. Johansson, M. Soto Thompson, M. Stenberg, C. af Klinteberg, S. Andersson-Engels, S. Svanberg and K. Svanberg, Feasibility study of a novel system for combined light dosimetry and interstitial photodynamic treatment of massive tumors, *Appl. Opt.* **41**, 1462-1468 (2002).